Coordination Chemistry Reviews 254 (2010) 1117–1134

Contents lists available at ScienceDirect

Coordination Chemistry Reviews

journal homepage: www.elsevier.com/locate/ccr

Review

Carbon nanotubes combined with inorganic nanomaterials: Preparations and applications

Haibin Chu, Li Wei, Rongli Cui, Jinyong Wang, Yan Li*

Beijing National Laboratory for Molecular Sciences, State Key Laboratory of Rare Earth Materials Chemistry and Applications, Key Laboratory for the Physics and Chemistry of Nanodevices, College of Chemistry and Molecular Engineering, Peking University, Beijing 100871, China

Contents

ARTICLE INFO

Article history:
Received 7 October 2009
Accepted 9 February 2010
Available online 17 February 2010

Keywords:
Carbon nanotubes
Inorganic nanomaterials
Composites
Catalysis
Energy conversion

ABSTRACT

The unique structure carbon of nanotubes endues them with superior electronic, optoelectronic, mechanical, and chemical performance. When combining with inorganic nanomaterials, the resultant composites show additional properties and broader applications. This review summarizes the handling of carbon nanotubes, the preparation of inorganic nanomaterial/carbon nanotube composites, and the application of such composites in a wide variety of fields.

* Corresponding author. Tel.: +86 10 62756773; fax: +86 10 62756773.
E-mail address: yanli@pku.edu.cn (Y. Li).

0010-8545/$ – see front matter
doi:10.1016/j.ccr.2010.02.009

1. Introduction

Carbon nanotubes (CNTs) are important carbon-based materials. A single-walled CNT (SWCNT) can be considered as a seamless cylinder formed by rolling a graphene sheet and a multi-walled CNT (MWCNT) is composed of a series of concentric SWCNTs with the inter-tube distance of ~0.34 nm. This unique structure endow CNTs with various superior properties, for example, low density, very high stabilty, outstanding tensile strength and resilence, good current carrying capacity and heat transmission ability, and extraordinary electronic behavior (can be either metallic or semiconducting depending on the rolling manner of graphene sheet) [1,2]. Owing to their excellent properties, CNTs have been intensively studied and have attracted wide attention in the last decade [3–10].

Inorganic nanomaterials, including elementary substances and compounds with great diversity, are an important family of nanomaterials with abundant properties in optics, electronics, magnetics and catalysis. The property of inorganic nanomaterials can be further tuned by varying their composition, structure and morphology [11].

Composite materials based on CNTs and inorganic nanomaterials integrate the unique characters and functions of the two types of components and may also exihibit some new properties caused by the cooperative effects between the two kinds of materials [12–16]. Therefore, these composte materials have shown very attractive potential applications in many fields. This review summarizes the handling of CNTs, the preparation of CNT-based nanocomposites, their properties and applications in catalysis, energy conversion, sensor, analysis, etc.

2. Preparation and handling of carbon nanotubes as supports for inorganic nanomaterials

The preparation of high purity CNTs and the dispersion of CNTs in proper media are essential for the synthesis of CNT-based composites. In this section, a brief discussion about the progress in preparation and handling of CNTs is made.

2.1. Preparation of carbon nanotubes

CNTs have been produced by various kinds of strategies. Arc discharge [17,18], laser ablation [19], and chemical vapor deposition (CVD) [20–23] are the most widely used techniques. However, the large-scale production of high quality CNTs is still a challenge. Compared with the other two methods, CVD is an economic pathway and is easily scaled-up to batch-scale production. Methane, ethane, ethylene, acetylene, and ethanol can all be used as the carbon source. The carbon sources are catalytically decomposed by either plasma irradiation (plasma-enhanced CVD, PECVD) [20,22] or heat (thermal CVD) [21,23] and then nucleated by the catalyst nanoparticles to form CNTs. The plasma used in PECVD is usually generated by hot filaments (HF) [20] or by electrical discharge at different frequencies (DC, RF, and MW) [24].

It is generally accepted that the CNTs grow via a vapor–liquid–solid (VLS) mechanism. Catalyst plays an important role in the CVD synthesis of CNTs [23]. The yield and quality of the products depends greatly on the composition, morphology and property of catalysts. Fe, Co, Ni and their alloys are the traditionally used catalysts. Recently it has been found that Cu, Pd, Au, Pb, and even Al and Mg can all be used to catalyze CNTs' growth [25–29]. The design of CVD process is also very important. For example, the preparation can be easily scaled-up by employing a "two-furnace" CVD method [30]. Fluidized-bed CVD [31] method can improve carbon conversions and thus benefit the formation of CNTs. The high-pressure CO conversion (HiPCO) process [32,33] has been commercialized to supply a large quantity of SWCNTs for research and development using SWCNTs as materials.

Using the CVD method, not only CNTs in bulk form are produced, but also CNTs, especially SWCNTs, on substrates can be synthesized by controlling the growth conditions [34–48]. SWCNTs directly grown on substrates normally have fewer impurities and are superior for in situ study on the loading of inorganic nanomaterials on nanotubes as well as the property of the resultant composites. The orientation of grown SWCNTs can be precisely controlled by external electric field [37,38], gas flow [39,40] or surface lattice of the substrates [41–43]. The density of SWCNTs can be controlled by selecting different catalysts or substrates [44–47]. Even pure semiconducting SWCNTs can be grown by utilizing quartz as substrate and methanol and ethanol as the carbon source [48]. Though tremendous progress has been made in growing SWCNTs, there are still many challenges in growing SWCNTs especially the control of chirality.

2.2. Purification and dispersion of carbon nanotubes

Generally, the carbon nanotubes as-prepared are grown as mixtures of carbon nanotubes and impurities such as amorphous carbon, metal catalyst particles and carbon nanoparticles. These impurities significantly influence the properties of CNTs and limit their applications. Consequently, development of economical purification methods has become an important issue to the development and practical applications of the carbon nanotubes. A commonly used purification approach consists of two steps. The thermal or acid oxidation treatment on raw carbon nanotubes can effectively remove the amorphous carbon, carbon nanoparticles and carbon layers coated on the metal particles [49,50]. The following acid refluxing treatment removes the residual naked metal-oxide particles [51]. This method is time consuming and has the disadvantage of low yield and damaging the nanotubes. Some extraordinary methods such as magnetic filtration, microwave irradiation, electrochemical oxidation, surfactant-assisted purification and $C_2H_2F_4$ or SF_6 treatment have shown higher efficiency in removing the contaminants in the CNT samples and are less damaging to the nanotube structure [52–55].

Due to the strong π–π stacking interactions between the neighboring CNTs, they tend to aggregate into bundles, making it very difficult for them to be dispersed in water and organic solvents. Their insolubility has become a great obstacle to the manipulation and application of CNTs. Dispersing nanotube at the individual nanotube level is critical for a better performance of carbon nanotubes in most applications, especially the preparation of CNT-based composites. Therefore, many strategies have been explored to improve the solubility of CNTs in solvents. They can be classified mainly into two types, one is the sidewall covalent functionalization, and the other is the noncovalent modification using guest molecules as solubilizers.

By sonication in mixtures of sulfuric and nitric acids or sulfuric acid and hydrogen peroxide, carbonyl and carboxylic groups can be introduced onto the nanotubes [56]. This is one of the most prevalently used covalent modification methods. The modified CNTs can be further functionalized by esterification or amidation reaction [57,58]. Other methods such as carbene cycloaddition, diazonium reaction and grafting of polymers have also been successfully used in the functionalization of CNTs [59,60]. The covalent methods convert the carbon atom hybridization from sp^2 to sp^3, leading to a disruption of electronic structure of CNTs.

The noncovalent modification methods, such as polymer and DNA wrapping, π–π stacking interactions with aromatic molecules and surfactant-assisted dispersion, are based on van der Waals or π–π stacking between CNTs and solubilizer molecules [61–64]. The noncovalent strategy offers the advantage of remarkably improving the CNTs' solubility without disrupting the electronic structure of the tubes. Therefore it is more attractive than the covalent method for the maintenance of pristine structure and properties of CNTs.

SWCNTs can be directly dispersed in the imidazolium-based ionic liquids simply by mechanical milling. The concentration of SWCNTs can be as high as 1 wt%, which is remarkably higher than that of conventional covalent and noncovalent approaches [65]. The prosperities of SWCNTs are well preserved, since only weak van der Waals force exists between SWCNTs and ionic liquids [66,67]. Therefore, imidazolium-based ionic liquids are superior solvents for the handling of CNTs [66,67].

3. Strategies for preparing inorganic nanocrystal/carbon nanotube composites

Inorganic nanocrystals comprise inorganic structural units such as nanoparticles, nanorods, nanowires, and nanotubes as well as complex/hierarchical inorganic nanostructures based on the aforementioned simple structural units. Due to their unique characteristics such as quantum effect, small size effect, and surface effect, inorganic nanocrystals have excellent electronic, optical, magnetic, and catalytic properties, and thus exhibit powerful applications in chemistry, physics, material science, biology, and medicine [68].

As reviewed in the former publications, numerous synthetic methodologies have been developed for the preparation of inorganic nanocrystal/CNT composites [12–16]. However, most papers report the preparation of inorganic nanocrystals supported on bulk CNTs. Up to now there are only a few papers reported the preparation of inorganic nanocrystals supported on surface-grown CNTs. The strategies for site-specific preparation of inorganic nanocrystals on CNTs are even fewer. In this review, besides the preparation of nanocomposites based on CNTs in bulk form, we also focus much on the recent advances in the controlled decoration of inorganic nanocrystals on surface-grown SWCNTs.

3.1. Strategies for preparation of inorganic nanocrystals supported on bulk CNTs

Many methods have been exploited for the preparation of inorganic nanocrystals supported on bulky CNTs. These methods can be divided into two categories. One is to prepare nanocrystals in advance and then assemble them with CNTs. Another is to form nanocrystals directly on CNTs.

3.1.1. Assembling inorganic nanocrystals with bulk CNTs

Inorganic nanocrystals can be connected to bulk CNTs via covalent bonding [69], electrostatic interaction [70,71], π–π stacking [72], hydrophobic interaction, or hydrogen bonding [73]. Binary, ternary, or even quaternary CNT-based nanocomposites of inorganic nanocrystals and CNTs can be thus prepared. For instance, six different multi-phase nanocomposites, TiO_2/CNTs, Co_3O_4/CNTs, Au/CNTs, Au/TiO_2/CNTs, TiO_2/Co_3O_4/CNTs, and Co/CoO/Co_3O_4/CNTs have been prepared under either sonication or simple mechanical stirring condition via a similar step-by-step self-assembly approach using pre-synthesized nanoparticles as building units [74].

The nanocrystals are synthesized before assembling with CNTs. Therefore it is much easier to control both the size and morphology of the nanocrystals because there are already numerous methods developed for the preparation of inorganic nanocrystals with controlled size and morphology. However, loading efficiency of nanocrystals onto unmodified CNTs is typically not very high. By functionalization or wrapping the CNTs with certain "gluing molecules" may result in higher loading of nanocrystals on CNTs. The types of surface groups of CNTs play key role in the interaction with the preformed inorganic nanocrystals. Pan et al. investigated the effects of CNTs with different surface groups on the luminescence properties of mercaptoacetic acid-capped CdSe quantum dots. They found that the binding constant for amine terminated CNT is much higher than that of carboxyl- and hydroxyl-terminated CNTs [75].

The performance of the composites might deteriorate because of the structural damage to the CNTs during the pre-modification and the electrical, mechanical, and optical properties of the nanotubes might be somewhat affected [12,76,77]. Therefore, the modification strategy must be carefully designed to avoid excessive interruption to the structure and property of CNTs.

3.1.2. Direct formation of inorganic nanocrystals on bulk CNTs

Inorganic nanocrystals supported on bulk CNTs can be prepared by adsorbing precursors physically or chemically on the outer walls of CNTs and subsequent reactions [78]. However, as-prepared CNTs normally lack sufficient binding sites to adsorb precursors of inorganic nanocrystals, which usually results in low loading efficiency of nanocrystals or aggregation and poor dispersion of nanocrystals at high loading. More binding sites, such as defects and functional groups (e.g., hydroxyl, carbonyl, carboxyl groups), can be introduced into CNTs by treating with acid, ultrasonication, microwave irradiation or γ-ray irradiation [13,16]. These binding sites play different and multifold roles in the preparation process. The defects or functional groups on CNTs may only act as nucleation sites or anchoring sites for the deposition of inorganic nanocrystals [79–81]. For example, Han et al. reported that SWCNTs treated with 40% HNO_3 realized a complete and uniform coating of tin oxide nanoparticles on the entire outer surfaces of SWCNTs when immersed in the solution of $SnCl_2$ [81]. The binding sites may adsorb one reaction precursor and then these precursors are further reacted by adding another reactant, e.g., reduced by adding some reducing agent such as H_2, $NaBH_4$, formaldehyde, ethylene glycol, and polyol [82,83]. Sometimes, the functional groups not only play the role of nucleation sites or anchoring sites, but also the reducing agents for metal nanocrystals formed on nanotubes. These methods offer highly effective approaches for generating various inorganic nanocrystal/CNT composites. However, the structure damage of CNTs caused by harsh treatment may impair the performance of the composites as already mentioned above.

In order to preserve the structure and pristine properties of the CNTs, some methods have been exploited to directly prepare inorganic nanocrystals supported on as-prepared CNTs. One of the earliest approaches is depositing inorganic nanocrystals on CNTs via evaporation, sputtering or thermal decomposition at high temperature [84–86]. Noble metals can be transformed into gas by thermal heating or sputtering. Then CNTs act as the nucleation templates for the gaseous metal atoms and metallic nanocrystals are deposited on CNTs. For instance, nanoparticle arrays of Au, Ag and Cu, and ultrafine (less than 5 nm in width) nanowires of Ti, Mo and Zr were formed within the grooves between tubes in CNT bundles. Moreover, the direction of cluster arrays and nanowires could be controlled by nanotube curvature. In another approach, organometallic compounds are easily decomposed at high temperature and they can be used as precursors to deposit metal nanocrystals onto CNTs [78]. Some other methods including atomic layer deposition (ALD) and chemical vapor deposition (CVD) which can be used similarly to decorate CNTs with semiconducting nanocrystals [87]. However, these processes should be performed strictly under oxygen-free environment to avoid damage to the structure of CNTs at the very high temperature.

Metal nanocrystals can also form directly on CNTs by electroless chemical deposition. $AuCl_4^-$ and $PtCl_6^{2-}$, which have relative high reduction electrode potential, are reduced by CNTs and form gold and platinum nanoparticles directly on CNTs [88,89]. The size of the metal nanoparticles decorating the CNTs can be varied by adjusting the reactant concentration and reaction time. However, surfactants are normally used to disperse the CNTs in this process so that the nanocrystals produced can be uniformly deposited onto the CNTs [88,89]. This electroless chemical deposition method is feasible only to metals with very high reduction potential, for example, noble metals.

The electrochemical deposition offers the approach for depositing more kinds of inorganic nanocrystals on bulk CNTs [14,15]. In a typical electrochemical deposition process, CNTs should be first transferred onto the working electrodes of electrochemical cells. Several parameters such as applied voltage, reaction time and reactant concentrations can be varied to control the size and the amount of loading of the inorganic nanocrystals. Other factors such as the preparation methods of CNTs, pretreatment and the conductivity of CNTs also play key roles in controlling the size of the nanocrystals on CNTs. The nanocrystals in the composites prepared by this method typically have large diameters. For instance, Wang et al. used the CNTs grown on carbon papers as the support for the electro-deposition of platinum nanoparticles and the average diameter of the resultant particles on CNTs is ~25 nm [90].

Wai's group [91,92] and Liu's group [93,94] developed an alternative approach to synthesize inorganic nanocrystal/CNT composites using supercritical fluids. Employing the unique properties such as low viscosity, high diffusivity, near-zero surface tension of supercritical fluids, not only the morphology and structure of metal or metal-oxide nanocrystals decorated on CNTs can be effectively controlled, but also some special nanostructures are prepared by this method. For example, Ye et al. found that ~10% of the total number of CNTs were filled with metal nanowires when they prepared metal nanoparticle/CNT composites by reducing metal precursors of Pd, Ni and Cu with hydrogen in supercritical CO_2 [91]. Such structures of inorganic nanocrystal/CNT composites are difficult to achieve using other solution-based synthetic methods.

Salt effect has been used to induce the selective heterogeneous nucleation and growth of nanoparticles on unmodified bulk CNTs [95]. Salts containing anions with weak coordination to metal ions such as sodium dodecyl sulfate, p-$CH_3C_6H_4SO_3Na$, $LiCF_3SO_3$, and $LiClO_4$ are used for this purpose. Evenly dispersed platinum nanoparticles with uniform size at an extremely high loading of ~50% have been successfully decorated on unmodified CNTs using this method [95].

Other methods such as sol–gel, hydrothermal or solvothermal and simple solution approaches are also effective for generating inorganic nanocrystals supported on unmodified CNT composites. In these processes, CNTs are very likely acting as templates to nucleate the nanocrystals and tune their particle size. The evidence for this argument is that the particles formed on CNTs are usually much smaller than those on graphite or active carbon [96]. However, there is an exceptional example. Larger CeO_2 nanoparticles are formed in the presence of CNTs [97]. This is due to the redox reaction between the CeO_2 nuclei and CNTs under the hydrothermal conditions. The reduction of Ce(IV) to Ce(III) by CNTs tend to dissolve the formed small CeO_2 nanoparticles and the re-crystallization process facilitates the formation of larger CeO_2 nanoparticles [97].

The existence of CNTs in the synthesis system not only influences the size of nanoparticles formed on CNTs, but also helps to tune the morphology of nanoparticles decorated onto CNTs. As shown in Fig. 1, CNTs are capable of triggering a morphological transformation of CdSe nanorods into pyramidal-shaped nanoparticles and a tight attachment to them during the synthesis of CdSe nanoparticles via the reaction between CdO and Se in the presence of octadecylphosphonic acid (ODPA), tri-*n*-octylphosphine oxide (TOPO) and tri-*n*-octylphosphine (TOP) [79]. In the first stage of the reaction, CdSe nanorods are formed and remain in solution capped with ODPA and TOP just as happens in the absence of CNTs (Fig. 1a). CNTs then act as coordinating ligands and attach CdSe nanorods via electrostatic interaction or the overlap of the delocalized π orbitals of the CNTs with the empty conduction band levels of Cd. In the second stage (Fig. 1b), the shape transformation starts with an etching process by ODPA and results in a Cd release beginning at the top of the nanorods. Obviously, the particles also slowly release Se in order to retain the proper stoichiometry (Fig. 1c). However, Se-rich surfaces are favorable under dynamic etching conditions, driving the particles into the finally observed morphology. The released ODPA promotes the transformation of the nanoparticles by an Ostwald ripening process (Fig. 1c and d). The right balance among several factors including a low passivated nanoparticle surface, particles with well-defined crystallographic facets, and interactions with an sp^2 carbon lattice facilitates the transformation of CdSe nanocrystals on CNTs [98].

Lee et al. reported evolution of the morphology of the single-crystalline copper sulfide (β-Cu_2S) nanocrystals grown in situ on acid-functionalized MWCNTs by the solvothermal method [99]. The morphologies of the Cu_2S nanocrystals are varied from spherical particles (average size ~4 nm) to triangular plates (average size ~12 nm) by increasing the concentration of the precursors. The lattice matching between Cu_2S and the MWCNTs is thought to play a key role in the growth of the Cu_2S nanocrystals on the surface of the MWCNTs.

The shape control of the inorganic nanocrystals formed on CNTs can also be realized through a seed-mediated growth approach. Heterostructures of ZnO nanorods on MWCNTs have been prepared using such a method [71]. First, the surfaces of the CNTs are coated in situ with ZnO nanocrystals of about ~7 nm by the reaction between zinc acetate and sodium hydroxide. These nanocrystals then serve as the seeds for further growth of ZnO nanorods in a seeded growth solution containing zinc nitrate and hexamethylenetetramine.

CNTs can also be used as a template to fabricate inorganic nanotubes if CNTs were completely covered with inorganic materials. In this case, CNTs are typically burned out during/after the formation of inorganic nanotubes. Here, introducing more binding sites (defects or functional groups) on CNTs is very important [100,101]. One approach is to adsorb precursors on the outer walls of CNTs and then transfer the precursors into target inorganic nanotubes by subsequent reactions. For example, a method including layer-by-layer (LBL) assembly of the precursors on CNT templates in combination with subsequent calcination has been developed to prepare porous In_2O_3 nanotubes [101]. LBL assembly in this method is based on the electrostatic attraction between the oppositely charged polyelectrolyte and metal ions. The highly distributed charges on the surface of CNTs modified with the polyelectrolytes ensure the formation of uniform and dense metal-oxide coating layers which can stand unbroken after burning CNTs. Metal-oxide nanotubes can also be prepared by first sputtering a thin layer of metal onto SWCNTs and then thermally oxidizing in air to form oxide nanotubes. Tin oxide nanotubes have been prepared using such a method [102]. The SWCNT templates can be completely removed by thermal oxidation above 600 °C. Similar methods such as ALD and CNT-template-assisted CVD can also be used to prepare metal-oxide nanotubes in a similar way [85,103]. For instance, metallic Ruthenium thin films can be deposited on CNT arrays by ALD using $Ru(od)_3$ (od = octane-2,4-dionate) at 300 °C. Ruthenium oxide nanotube arrays were then fabricated after the removal of CNT templates. Alternatively, Liu and co-workers developed a supercritical-fluid approach for fabricating α-Fe_2O_3 nanotubes by fully coating CNTs with continuous Fe_2O_3 nanoparticles from the decomposition of $Fe(NO_3)_3$ in a supercritical CO_2/ethanol solution, followed by the removal of the CNTs [104]. Besides, Rao et al. reported the fabrication of ZrO_2, Al_2O_3, V_2O_5, SiO_2, and MoO_3

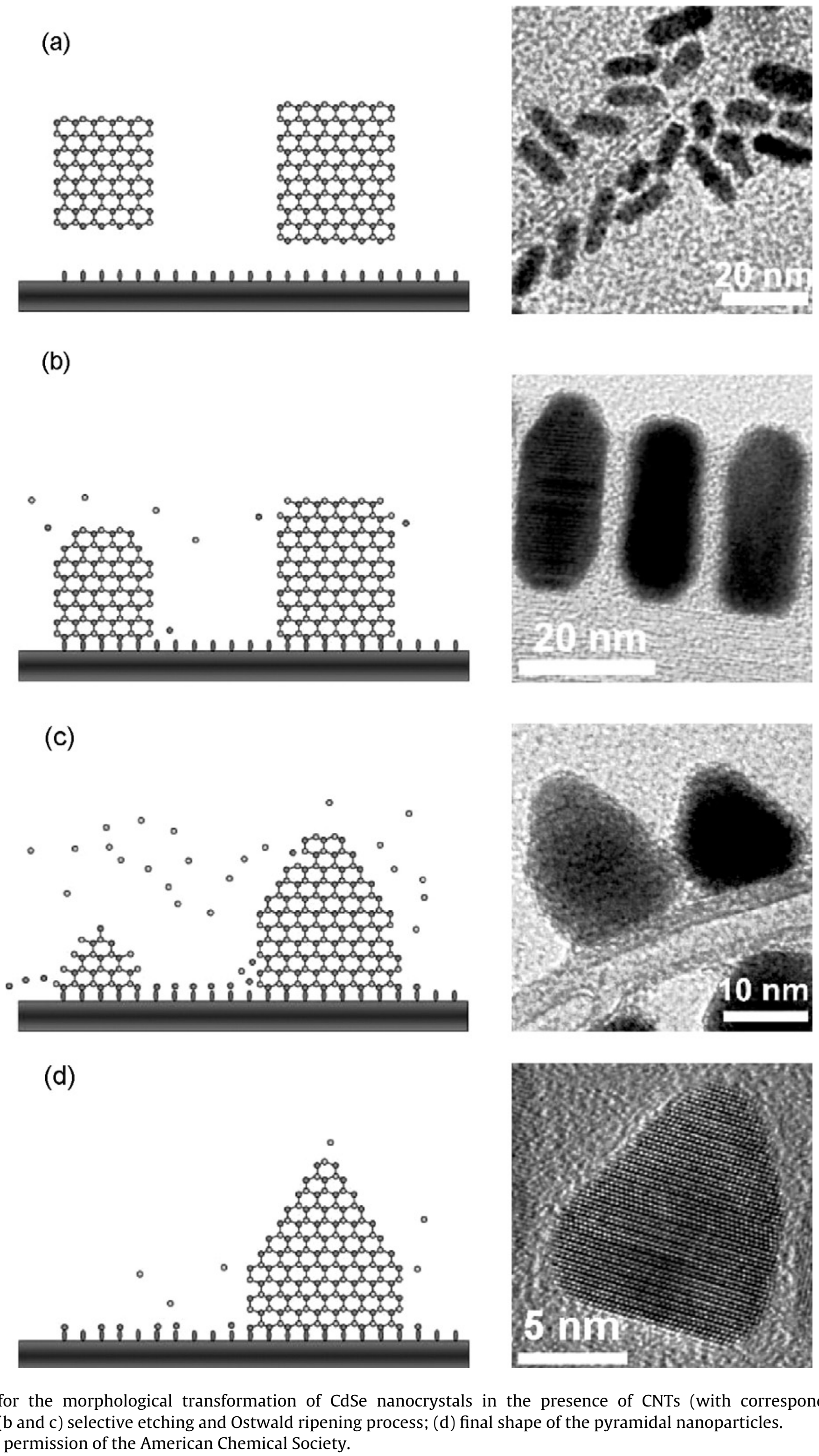

Fig. 1. Proposed mechanism for the morphological transformation of CdSe nanocrystals in the presence of CNTs (with corresponding typical TEM images). (a) Nanoparticle–CNT interaction; (b and c) selective etching and Ostwald ripening process; (d) final shape of the pyramidal nanoparticles.
Reproduced from Ref. [79] with permission of the American Chemical Society.

nanotubes by a sol–gel process using metal alkoxides as precursors and CNTs as templates in combination with subsequent calcination [105].

3.2. Strategies for preparation of inorganic nanocrystals supported on surface-grown CNTs

Compared with bulk inorganic nanoparticle/CNT composites, nanocomposites based on inorganic nanocrystals and surface-grown CNTs may have some unique properties and functions. Due to the low defect density, clean surface and intact structure, as-prepared surface-grown SWCNTs have potential applications in nano-electronics and optoelectronics [106,107]. SWCNTs with different diameter and helicity possess sharply different molecular structure and electronic band structure, which may result in completely different electronic and optoelectronic properties. Up to now, the detection of the molecular structure and electronic band structure of every individual SWCNT in a surface-grown sample

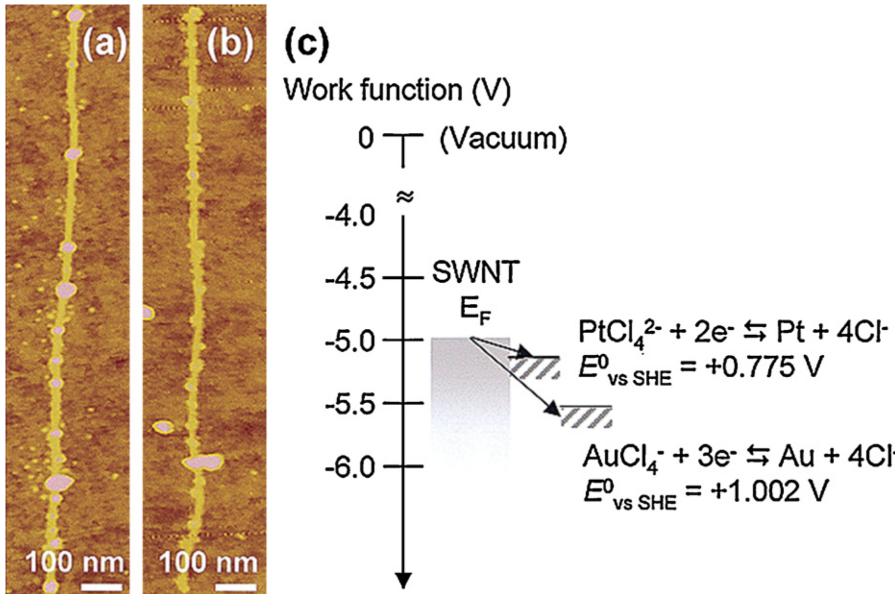

Fig. 2. Atomic force microscopic (AFM) images of metal nanoparticles formed on SWCNT sidewalls. (a) Au nanoparticles spontaneously and selectively formed on an individual SWCNT after immersion in Au(III) solution for 3 min. (b) Pt nanoparticles formed on a SWCNT after 3 min exposure to a Pt(II) solution. (c) Diagram showing the Fermi energy (EF) of a SWCNT, and the reduction potentials of Au(III) and Pt(II) species vs. SHE, respectively.
Reproduced from Ref. [115] with permission of the American Chemical Society.

remains a big challenge. The decoration of inorganic nanocrystals with surface-grown CNTs provides possibilities to explore CNTs' structure and properties with the help of the optical, electrical and magnetic functions of the nanocrystals. Moreover, because of the unprecedented low background current of the surface-grown SWCNTs when used as electrode materials [108], as well as their super high sensitivity towards electrochemical detection and chemical detection of species both in solution phase and gas phase [109],

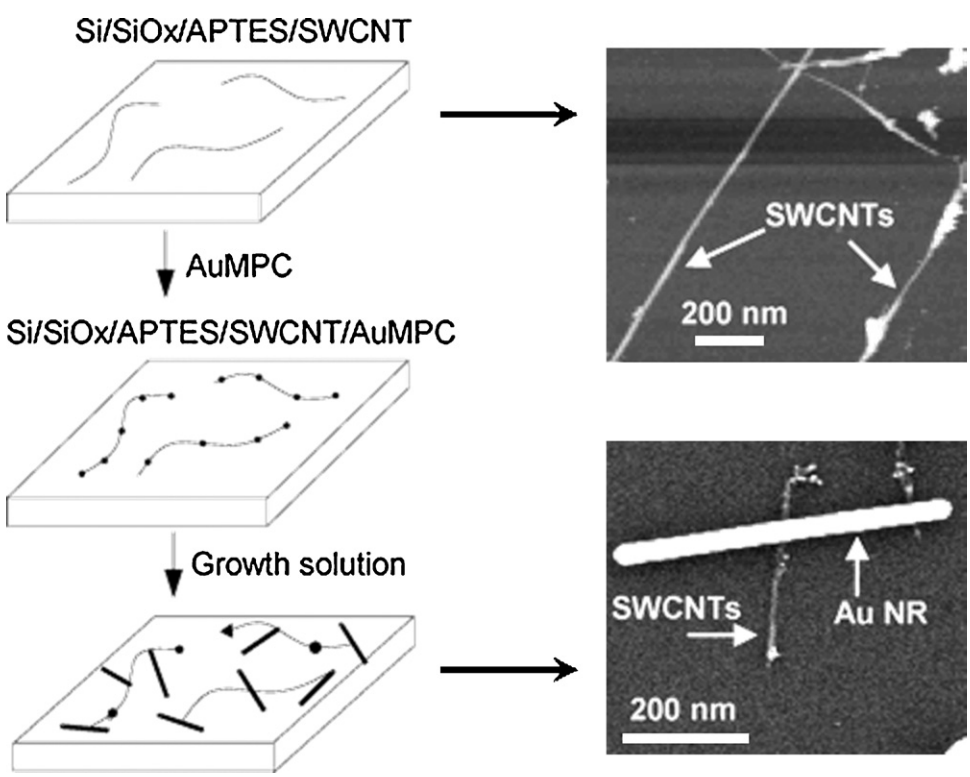

Fig. 3. Scheme showing the seed-mediated deposition of gold nanorods onto SWCNTs. First, SWCNTs are deposited onto (aminopropyl)triethoxysilane-functionalized Si/SiO$_x$. Second, the substrate is placed into a solution of monolayer-protected Au clusters (AuMPCs). Finally, the substrate is placed into a growth solution for 1 h. The top AFM image shows the SWCNT deposited on substrate. The bottom scanning electron microscopic (SEM) image shows a crossed Au nanorod/SWCNT junction formed using this procedure.
Reproduced from Ref. [116] with permission of the American Chemical Society.

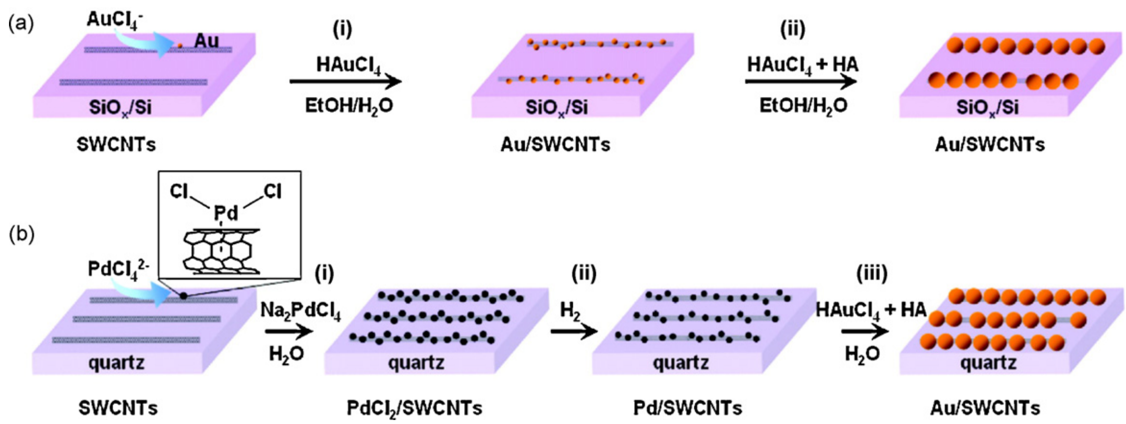

Fig. 4. (a) Scheme of the controlled decoration of gold nanoparticles onto SWCNTs based on gold seeds via gold seed decoration and subsequent seeded growth stages; (b) scheme of the controlled decoration of gold nanoparticles onto SWCNTs based on palladium seeds via $PdCl_2$ adsorption, H_2 reduction, and seeded growth stages.
Reproduced from Ref. [117] with permission of the American Chemical Society.

surface-grown CNTs are expected to be excellent sensors. However, the kinds of detected species are limited by the inherent electrical properties of CNTs. Fortunately, the decoration of inorganic nanocrystals onto CNTs not only enlarges the types of analytes for the sensors, but also enables the further increase of the detection sensitivity.

Surface-grown CNTs have some advantages over bulk CNTs for the decoration of inorganic nanocrystals. For instance, surface-grown CNTs are uniformly dispersed and well separated. Therefore, the dispersion of CNTs with the aid of surfactants is not needed before the decoration of inorganic nanocrystals and the intrinsic properties of CNTs can be effectively kept. However, preparing inorganic nanocrystals supported on surface-grown CNTs faces more challenges than those supported on bulk CNTs. The existence of substrates under CNTs limits the choice of preparation methods in two aspects. First, those methods which may degrade the substrates or lift the CNTs from substrates should be avoided. Second, the wetting property of the substrates restricts the choice of solvents. The strategy of assembling pre-synthesized inorganic nanocrystals onto CNTs which has been very successful in the modification of bulk CNTs is seldom adopted for as-prepared surface-grown CNTs because this strategy typically leads to a very low loading efficiency and poor selectivity of deposition nanocrystals only on CNTs. It is more difficult to control the size, morphology, distribution and selectivity of inorganic nanocrystals decorated on surface-grown CNTs than on bulk nanotubes. Furthermore, the application of surface-grown CNTs requires keeping the intrinsic structure and properties of CNTs as much as possible. Thus, covalent or noncovalent modification and any harsh treatment of the CNTs should be avoided if possible. Therefore, the efficient preparation methods for inorganic nanocrystals supported on surface-grown CNTs are limited.

3.2.1. Gas phase deposition [110–114]

Kong et al. have fabricated excellent hydrogen sensors by decorating SWCNTs with Pd nanoparticles via electron-beam evaporation over the substrates containing SWCNT devices [110]. Later, Star et al. used thermal or electron-beam evaporation to deposit Mg, Al, Ti, V, Cr, Mn, Fe, Co, Ni, Zn, Mo, Rh, Pd, Sn, W, Pt, Au, and Pb metals onto surface-grown SWCNTs, and tested gas sensing performance of every metal nanocrystal/SWCNT composite towards H_2, CH_4, CO and H_2S [113]. Besides, both Dai's group and Cronin's group have decorated surface-grown SWCNTs with gold or silver nanoparticles by electron-beam evaporation [111,114]. This class of methods is capable of controlling the size and covering density of metal nanocrystals on CNTs by varying the evaporation temperature, electron-beam energy and deposition time. However, the deposition of metal nanoparticles is homogeneous over the substrates and does not show any selectivity on CNTs.

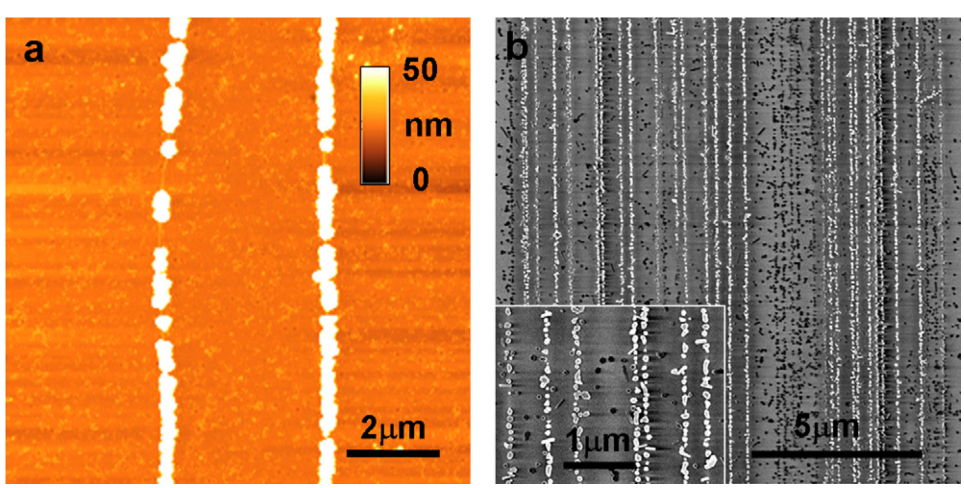

Fig. 5. (a) AFM topographical image of the gold/SWCNT composites obtained by seeded growth based on gold seeds. (b) SEM image of the gold/SWCNT composites obtained by seeded growth based on palladium seeds. Inset in (b) is the magnified image.
Reproduced from Ref. [117] with permission of the American Chemical Society.

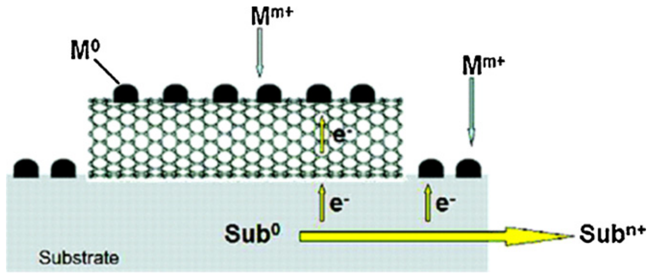

Fig. 6. Schematic illustration of metal nanoparticle deposition on carbon nanotubes via the substrate-enhanced electroless deposition process.
Reproduced from Ref. [119] with permission of the American Chemical Society.

3.2.2. Electroless deposition of metal nanoparticles on SWCNTs via oxidation–reduction reaction [19]

This method only works for the metals whose reduction electrode potentials are higher than that of CNTs. Noble metals such as Au and Pt have been deposited onto surface-grown SWCNTs with this method [115]. As shown in Fig. 2, Au and Pt nanoparticles can be spontaneously deposited on SWCNTs with very high selectivity when the surface-grown SWCNT samples are immersed into the corresponding salt solutions [115].

Fig. 3 shows the formation of gold nanorod/SWCNT heterojunctions through a two-step process [116]. First, monolayer-protected Au clusters with an average diameter of 1.6 nm adsorb onto SWCNTs via hydrophobic interactions. Second, these Au clusters act as seeds for the seeded growth of Au nanorods in the seeded growth solution containing $HAuCl_4$, cetyltrimethylammonium bromide (CTAB) and ascorbic acid.

Fig. 4 shows two routes to selectively decorate Au nanoparticles onto surface-grown SWCNTs with controlled size and interparticle distance [111]. The seeds are antecedently deposited on SWCNTs with high selectivity via the reduction of $HAuCl_4$ by SWCNTs (Fig. 4a) or the formation of stable complexes between $PdCl_2$ and SWCNTs (Fig. 4b). The following well-controlled seeded growth ensures the selective decoration of gold nanoparticles with controlled size and interparticle distance on SWCNTs (Fig. 5). The decorated nanoparticles align well along the SWCNTs.

Besides seeded process, noncovalent modification-mediated methods have also been used to decorate nanocrystals onto surface-grown SWCNTs. A solution-phase method has been designed to spontaneously form transition-metal nanoparticles on SWCNTs via noncovalent functionalization of 2,2′:6′,2″-terpyridine (Terpy) on SWCNTs [118]. The electron injection from Terpy into SWCNTs elevates the Fermi level of SWCNTs. Therefore, even transition metals whose salts have reduction potential lower than SWCNTs, such as salts of Ru, Cu, Zn and Sn, can still selectively deposit on Terpy-functionalized SWCNTs. Fig. 6 shows a substrate-enhanced electroless deposition to reduce metal ions with reduction potentials lower than that of CNTs into metal nanoparticles [119]. In this method, CNTs are supported on metal substrates of a redox potential lower than those of the metal ions which are then reduced to be metal nanoparticles onto CNTs. CNTs are not the reducing agent in this case and they only act as cathodes and templates for metal deposition from the corresponding metal salts. A large variety of metal nanoparticles, including Cu and Ag, have been successfully decorated on CNTs by this method.

3.2.3. Electrochemical deposition [113,120–130]

CNTs are typically grown on insulating substrates such as silica, quartz and sapphire. Therefore, metal electrodes should be fabricated on surface-grown CNTs to perform the electrochemical deposition (Fig. 7) [120–122]. The connected system consisting of CNTs and electrodes then acts as a working electrode for the electrochemical reduction of the metal precursors to metal nanoparticles selectively decorated onto CNTs. In this method, CNTs typically do not react with the metal salts but just act as molecular conducting wires and templates for the deposition of metal nanoparticles.

Noble metals such as Au, Ag, Pt and Pd can all be plated on the sidewalls of SWCNTs under direct potential control [113,120–130]. Importantly, both the size and number density of the metal nanoparticles decorated on SWCNTs can be varied by adjusting the potential and reaction time [122]. However, SWCNTs far away from the contacting electrodes or SWCNTs with poor conductivity are very difficult to be effectively decorated [120,125,128]. Moreover, due to the potential decrease along the SWCNTs away from the contacting electrodes, both the number density and diameter of

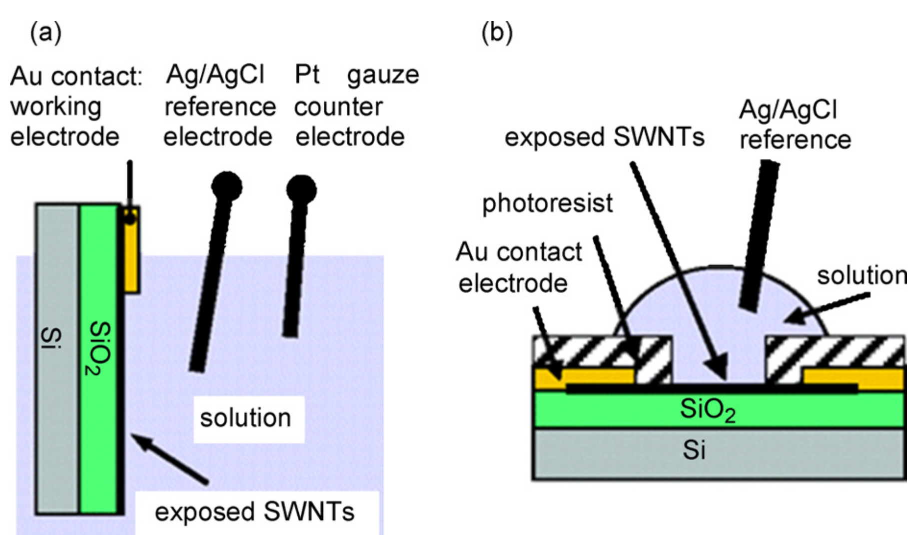

Fig. 7. Schematics of the setups used as working electrodes. (a) Electrode device 1 which consists of a Au band (200 μm in width, ca. 4 mm long) connected to a network of pristine SWCNTs; (b) electrode device 2, which uses a 20 μm × 400 μm area of high-density SWCNTs as the electrode, with the electrical contact insulated from the solution using a resist.
Reproduced from Ref. [120] with permission of the American Chemical Society.

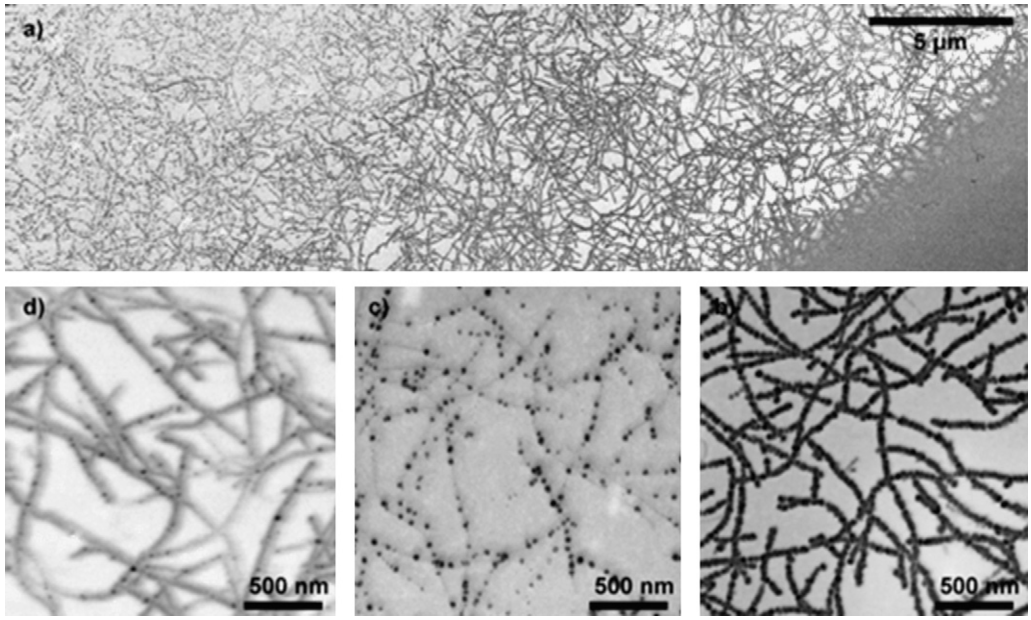

Fig. 8. SEM images showing (a) Pt deposited on SWCNTs, using electrode device 1, from a solution containing 2 mM K_2PtCl_6 in 0.5 M perchloric acid. A deposition potential and time of −0.4 V (vs. Ag/AgCl) and 30 s were used. The SWCNT network density was 6.8 μm SWCNT μm^{-2}. In the bottom right of the image is the Au contact electrode which was also exposed to solution. (b)–(d) are higher resolution SEM images: (b) close to, (c) ca. 15 μm from, and (d) further away (ca. 25 μm) from the contact electrode. Reproduced from Ref. [120] with permission of the American Chemical Society.

the nanoparticles vary along the tubes because of the difference of distance away from the contacting electrode (Fig. 8) [120,129].

Qian et al. report that the particle densities along all SWCNTs exponentially decrease with the increase of tube length [129]. Also, metallic and semiconducting SWCNTs (m-SWCNTs and s-SWCNTs), show obviously different electro-deposition behavior, i.e., the s-SWCNTs exhibit a remarkably faster decay rate compared to m-SWCNTs (Fig. 9). They believe that the different behavior of potential drop along nanotubes and electrochemical gating play dominant roles in the different electro-deposition behavior of m-SWCNTs and s-SWCNTs. Moreover, this electrochemical approach can be used as a simple strategy to identify m-SWCNTs and s-SWCNTs.

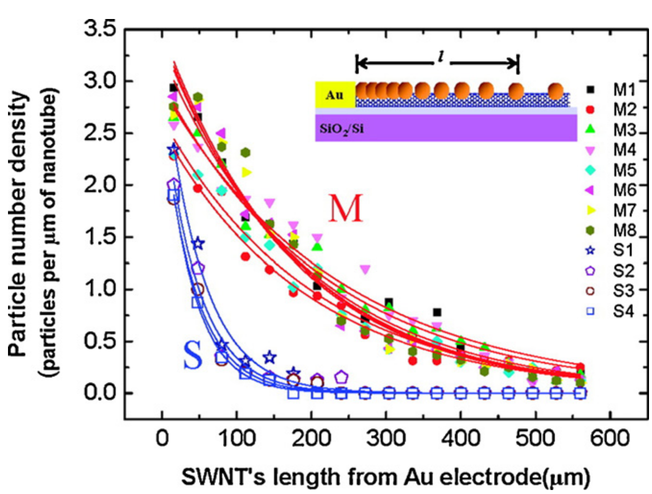

Fig. 9. Particle number density of 12 Ag-decorated SWCNTs with −0.6 V for 40 ms. They are denoted as M1-M8 for m-SWCNTs (solid marks) and S1-S4 for s-SWNTs (hollow marks). Solid curves are exponential decay fits of these data points. Reproduced from Ref. [129] with permission of the American Chemical Society.

3.3. Strategies for site-specific preparation of inorganic nanocrystals on CNTs

Site-defined preparation of inorganic nanocrystals on CNTs may find some unique applications. For instance, site-specific decoration of metal nanocrystals on CNTs allows the fabrication and positioning of microelectrodes on CNTs at nanoscale precision [123]. The deposited metal nanoparticles may also serve as active sites for site-defined modification or for growth of CNT-based mesostructures [116]. Besides, if the gold nanoparticles can be precisely positioned on the sidewalls of SWCNTs, the CNT-based single-electron transport behavior might be facilitated [131]. However, it remains a great challenge to deposit inorganic nanocrystals at preselected locations on CNTs; there are only a few reports on this subject.

A bipolar electrochemical method has been developed to selectively modify one end of the MWCNTs with gold nanoparticles (Fig. 10) [132]. A suspension of MWCNTs is filled into a capillary containing an aqueous $HAuCl_4$ solution. Then a high electric field (e.g., 30 kV) is applied to orient and polarize the individual tubes, and electrochemical reduction of gold nanoparticles onto each CNT takes place at one end while water oxidation occurred at the other end (Fig. 11). The size of the formed metal clusters is proportional to the potential drop along the nanotube and is also determined by the reaction time. There is another report which uses microwave fields to induce strong polarization potentials at m-SWCNTs' extremities and thus initiates the electrochemical reduction of $HAuCl_4$ [133]. Gold nanoparticles and sheaths deposit regioselectively at the SWCNT tips via this approach. While the above two methods enable the site-specific decoration of inorganic nanocrystals at the end of the nanotubes that are in bulk solution, they are probably not suitable for the site-defined preparation of nanocrystals on surface-grown nanotubes.

A precise control to the site-specific deposition of nanoparticles on CNTs can be realized with the help of focused-ion-beam (FIB) technique. FIB can site-selectively create functional groups such as O=C–O, C=O and C–O–H moieties on MWCNTs, which

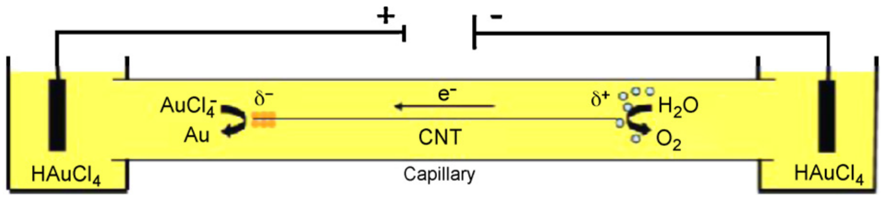

Fig. 10. Capillary filled with an aqueous CNT/$AuCl_4^-$ suspension dipping in the two reservoirs of a capillary electrophoresis setup. A high electric field is applied, leading to the polarization of the individual nanotubes, thus triggering different electrochemical reactions on either end.
Reproduced from Ref. [132] with permission of the American Chemical Society.

are subsequently used to trap gold nanoparticles onto the tubes assisted by poly(diallyldimethylammonium) chloride (PDADMAC) [134]. This approach can realize the position resolution as small as 5 nm. However, this method needs state-of-the-art technique and the condition is very harsh, thus it is not suitable for non-destructive modification of SWCNTs. Electron-beam lithography (EBL) can also be used for the site-defined deposition of nanoparticles on CNTs. Quinn and Lemay have deposited one single platinum nanoparticle at the exposed end of each SWCNT with a method combined by micro-fabrication and electrochemical deposition [123]. First, the exposed ends of SWCNTs are formed by using EBL on the poly(methyl methacrylate) (PMMA) coated surface-grown SWCNTs. Then the nanotubes serve as nanoscale wires and corresponding ends act as nanoscale templates for the deposition of metal nanoparticles.

Comparing with FIB and EBL, scanning probe lithography (SPL) is more flexible because it is much easier to control the movement of the scanning probe. Gold nanoparticles can be moved onto the nearby SWCNTs by a scanning probe to fabricate single-electron transistors and single-electron detectors [135,136] or to study the surface-enhanced Raman spectroscopy (SERS) [137]. As shown in Fig. 12, Tong et al. have used atomic force microscope (AFM) to

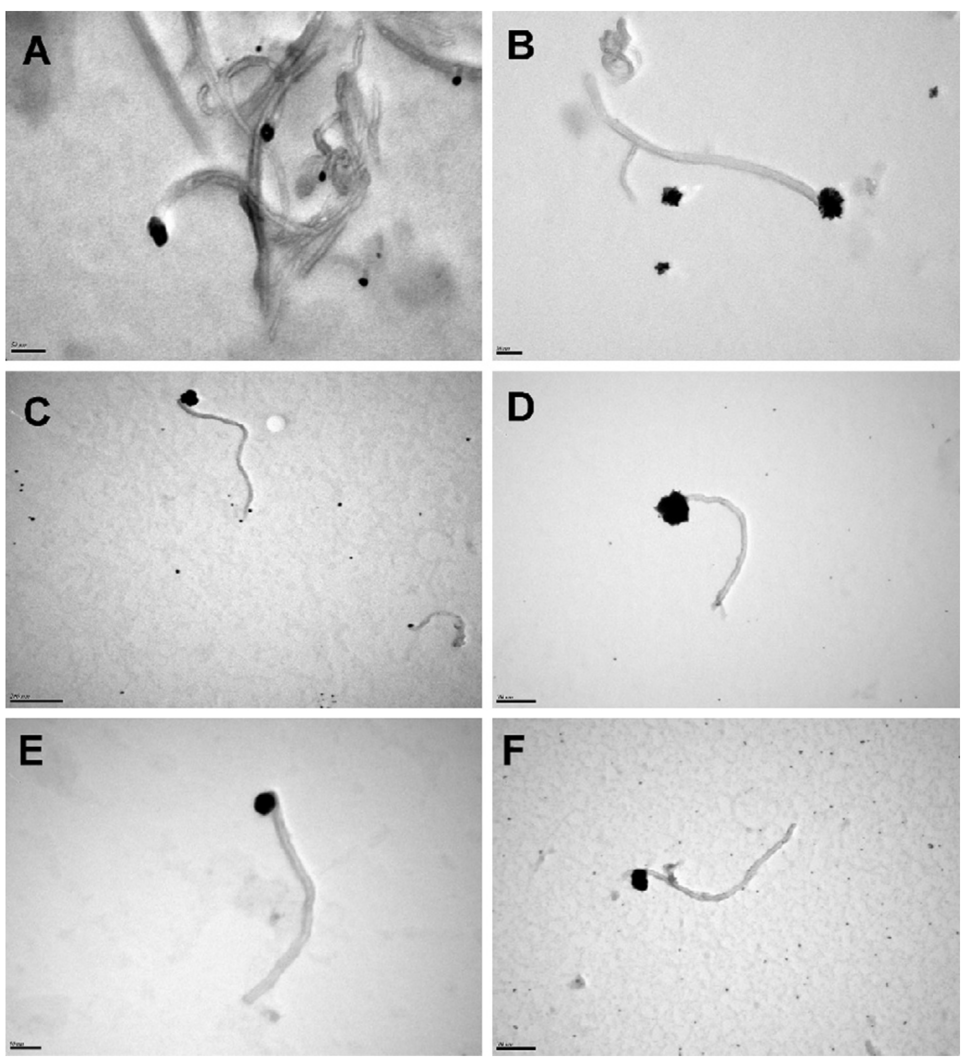

Fig. 11. Examples of CNTs modified on one end with a gold nanoparticle deposited in a solution of 1 mM $HAuCl_4$ by bipolar electrochemical reduction in a 45 cm long capillary under 30 kV. (Scale bar is 200 nm in (c), 100 nm in (d and f), 50 nm in (a, b, and e).)
Reproduced from Ref. [132] with permission of the American Chemical Society.

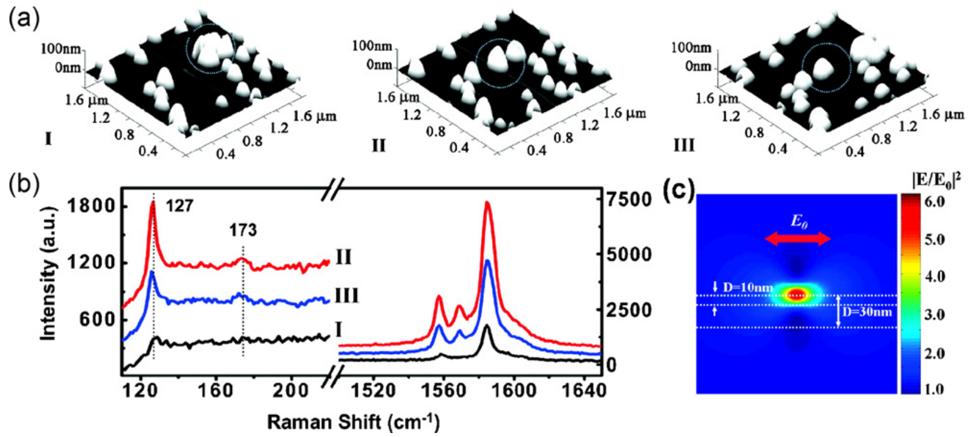

Fig. 12. AFM images of a manipulated gold nanoparticle (GNP) and the corresponding Raman spectra. (a) AFM images (1.8 μm × 1.8 μm) of a single GNP and a SWCNT at distances of ~200 (I), ~10 (II) and ~30 nm (III), respectively. (b) The corresponding Raman spectra for I (black), III (blue), and II (red) in panel (a). (c) The electric field profile on the substrate under the GNP simulated by the generalized Mie theory. The laser polarization is parallel to the axis of the SWCNT.
Reproduced from Ref. [137] with permission of the American Chemical Society.

manipulate the distance between the gold nanoparticle and the SWCNT, and then investigate the effect of the distance on the SERS intensity of the SWCNT [137].

One of the limitations of this strategy is the difficulty in handling nanoparticles smaller than 10 nm by scanning probe manipulation [135]. Whereas the small size of the nanoparticles is essential for building room temperature single-electron transistors [135]. Moreover, this method often results in poor contact between nanoparticles and SWCNTs, which may influence the single-electron transport behaviors of the devices [136]. However, the contact can be improved by post-treatment. Dockendorf et al. employed a fountain-pen method to deposit the nanoink of gold nanoparticle suspension on the area where the CNT contact the metal pad [138]. After annealing and sintering of the ink pattern, the contact resistance between the CNT and the metal pad is effectively decreased. However, the outer diameter of the micropipette tip is typically a few micron meters, therefore the size of the gold pattern formed by this method is typically at the micrometer scale.

Other than manipulation, the SPL-based direct preparation of nanoparticles on SWCNTs offers more feasible routes. The site-specific decoration of Au nanoparticles on any selected sites of SWCNTs has been realized using AFM dip-pen nanolithography (DPN) (Fig. 13) or electrochemical DPN (E-DPN) (Fig. 14) [139]. By adjusting the writing velocity, tip voltage bias and the times of seeded growth process, Au nanoparticles with sizes from several nanometers to hundreds of nanometers are controllably deposited on SWCNTs. Besides, this method provides a route for in situ monitoring the deposition of Au nanoparticles.

4. Applications of inorganic nanocrystal/carbon nanotube composites

4.1. Catalysis

CNTs have been used as support for the dispersion and stabilization of catalyst nanoparticles, due to their high specific surface areas, electrical conductivities, and chemical stability. The catalytic behavior of CNT–supported metal nanoparticles including Pt, Pd, Au, Ag, Rh, Ru, Co and Ni have been extensively studied. The CNT–supported metallic catalysts show excellent catalytic activities for many organic reactions [12,13,140].

The first report on the catalytic application of metal nanoparticles/CNT composites appeared in 1994. Ajayan et al. described the use of Ru NP/SWCNT composites in heterogeneous catalysis. The Ru nanoparticles are well dispersed on the surfaces of nanotubes, and show higher selectivity for cinnamyl alcohol (up to 92%) than Ru on Al_2O_3 (20–30%) in the liquid-phase hydrogenation of cinnamaldehyde. The unusual catalytic behavior is ascribed to the difference in metal–support interaction [78]. However, the nature of the interaction between metal and CNTs is unclear. From then on, the strong interaction between the metals and CNTs has been frequently mentioned in different reports [141–145]. 1 wt% Rh/CNTs exhibits higher activity for NO decomposition than 1 wt% Rh/γ-Al_2O_3 [144]. The electron transfer between CNTs and metal is believed to prevent rhodium from being oxidized, therefore larger amount of metallic Rh presents in the CNT–supported catalysts and hence results in the higher catalytic activity of Rh/CNTs [144].

In addition, CNTs do not have micropores, into which small metal nanocrystals may sink and become inaccessible. This definitely is an advantage for CNTs using as catalyst supports. The absence of micropores may also modify the adsorption properties and residence time of the reactants and products on CNTs [140], ultimately improves the selectivity of the catalyst. For example, the Pd/MWCNTs exhibits higher selectivity towards the C=C bond hydrogenation compared with Pd/activated charcoal (AC) (Fig. 15) [143]. This is attributed to the faster desorption of the C=C hydrogenated products from the active sites. Whereas on the Pd/AC, the cinnamaldehyde adsorbs in a different way, leading to the almost simultaneous hydrogenation of C=O and C=C bonds.

Besides use as the supporting materials, CNTs may also act as templates in tailoring the size of metal particles, especially for those filled in the CNTs [141–143,145,146]. The small space within the channels of CNTs can restrict the growth of the particles inside, which is helpful for the maintenance of optimum particle size. Moreover, the unique electronic structure, the tubular morphology and the high aspect ratio of MWCNTs may provide a special reaction environment within the CNT inner channels. The tubular inner channels have confinement effect on the gases or liquids trapped inside, which can increase the density of reactants [147], and hence create a locally higher pressure. This effect leads to a striking enhancement on the catalytic activity of Rh particles confined inside nanotubes for the conversion of CO and H_2 to ethanol [142]. As shown in Fig. 16, the formation rate of ethanol catalyzed by Rh within the CNT channels is an order of magnitude higher than that by Rh supported on the outer walls of CNTs.

In addition, the carbon wall might influence the morphology of the inorganic nanocrystals as mentioned above. For example, NiS_2 particles formed inside the MWCNTs are faceted with a peculiar orientation along the tube axis, which is completely different from that observed on traditional supports [141]. Therefore using

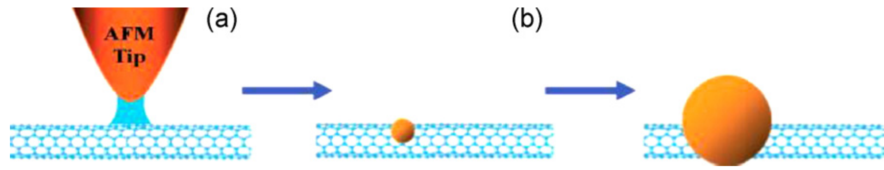

Fig. 13. Schematic showing the site-specific deposition of a gold nanoparticle on a SWCNT by DPN (a) and subsequent seeded growth (b).
Reproduced from Ref. [139] with permission of the American Chemical Society.

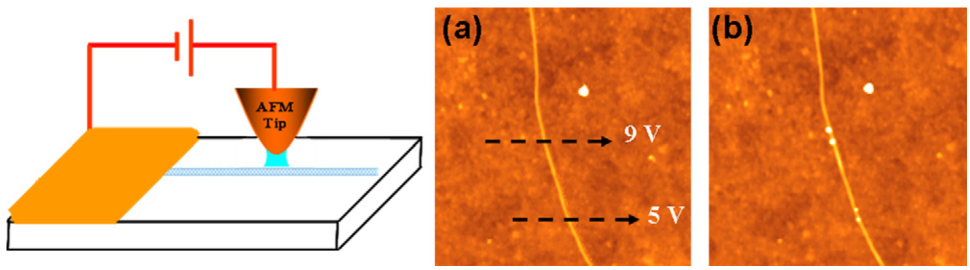

Fig. 14. Electrochemical DPN for direct deposition of gold nanoparticles on ultralong SWCNTs. Topographical images of the carbon nanotube before (a) and after (b) the E-DPN process in which the AFM tip was translated across the nanotube along the two dashed lines under different tip voltage bias. The heights of the four deposited nanoparticles are 4.5, 4.4, 1.3, and 2.2 nm, respectively.
Reproduced from Ref. [139] with permission of the American Chemical Society.

CNTs as templates may obtain metal nanoparticles with special morphologies and structures and hence unusual catalytic activities.

Of course, the catalytic activity and selectivity of metal/CNT composites depend greatly on the structure and surface property of both CNTs and the loaded catalyst particles as well as the content of the catalysts [145,148]. Oxygenated groups are usually created on the surface of CNTs by the HNO_3 treatment, which can act as the anchoring sites for the catalyst precursors, so as to improve the dispersion of the catalysts [148]. Recently, Wang and co-workers found that Ru/CNTs is a highly selective Fischer–Tropsch catalyst for the formation of C_{10}–C_{20} hydrocarbons [149]. It was found that the Ru/CNT catalyst with a mean Ru size of approximately 7 nm and CNTs pretreated with concentrated HNO_3 exhibits the best C_{10}–C_{20} selectivity. The unique adsorbed hydrogen species and the acidic functional groups on CNT surfaces may both play roles in mild hydrocracking of heavier hydrocarbons to C_{10}–C_{20}.

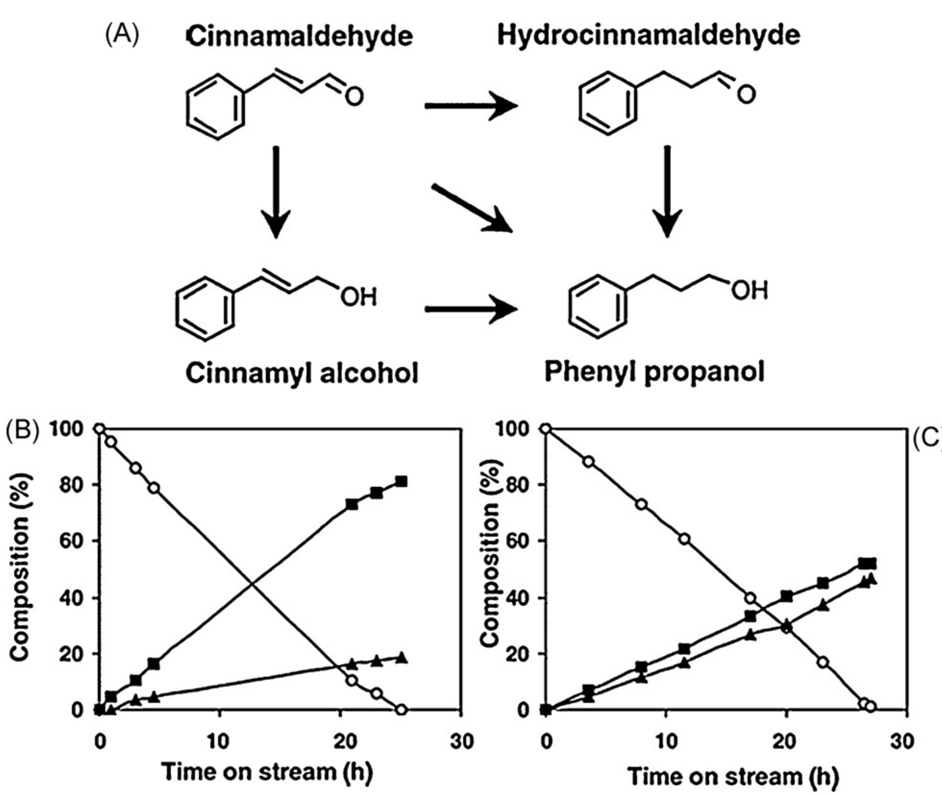

Fig. 15. Reaction pathways in the hydrogenation of cinnamaldehyde (a) and catalytic activity for the selective hydrogenation of cinnamaldehyde into hydrocinnamaldehyde over Pd/MWNT (b) and Pd/AC (c). (○) Cinnamaldehyde, (■) hydrocinnamaldehyde, and (▲) 3-phenylpropanol.
Reproduced from Ref. [143] with permission of Elsevier.

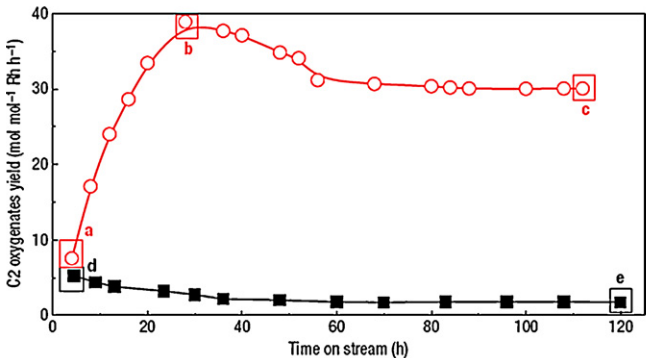

Fig. 16. C_2 oxygenate formation activities as a function of time on stream. Reaction temperature: 320 °C.
Reproduced from Ref. [142] with permission of the Nature Group.

Inorganic nanomaterials especially nanoscaled metals supported on CNTs present unusual catalytic behavior comparing with those loaded on active carbon and other normally used supports and show great potential in future applications. However, the mechanism of the unique catalytic property of CNT–supported catalysts is not very clear yet. Therefore the rational design of catalysts with desired catalytic property is still a dream. Great efforts are still needed to study the surface modification of CNTs, the controlled preparation of nanoscaled catalysts on CNTs, and the interactions between CNTs and the catalyst particles. These informations will be very important for exploring the mechanism of processes catalyzed by CNT–supported catalysts.

4.2. *Energy conversion*

The unique electrical and electronic properties, a wide electrochemical stability window, the high surface area, and the one-dimensional geometric structure enable CNTs superior electrode materials for use in energy conversion devices. Inorganic nanomaterials often act as the functional materials in the energy conversion devices. For example, inorganic nanoparticles are used as catalysts in fuel cells and to facilitate the generation of electron–hole pairs in solar cells. Therefore, the combination of CNTs with inorganic nanomaterials has shown great promise in energy conversion processes. In this part, recent progress in the application of inorganic nanomaterial/CNT composites in fuel cells for chemical energy conversion and solar cells for solar energy conversion is summarized.

4.2.1. *Fuel cells (chemical energy conversion)*

A fuel cell is a kind of device that can directly convert chemical energy of fuels such as hydrogen and methanol into electricity. The conventional direct methanol fuel cells (DMFCs) and proton exchange membrane fuel cells (PEMFCs) normally use carbon black-supported Pt as the catalyst for electrode reactions [140,150–152]. The energy crisis has pushed us to exploit fuel cells with low pollution and high performance. One of the most important issues in the research of fuel cells is to reduce the cost of the electrodes together with the improvement of the catalytic activity [140,150]. From this point, CNTs are promising to replace the commercialized carbon black as the catalyst supports for the fuel cells because they can dramatically enhance the catalysis utilization and the activity and stability of the catalytic noble metals. In comparison with commercialized carbon black support, CNTs have higher electronic conductivity, larger specific surface area, better mechanical and thermal properties and stronger anti-oxidation ability. Furthermore, the unique tubular structure of CNTs enables the controlled dispersion of metal particles on the outwalls of CNTs, while carbon black has a large ratio of micropores smaller than 2 nm, into which Pt nanoparticles may sink and Pt utilization may be reduced.

The CNT–supported Pt nanoparticles have shown remarkably enhanced behavior. Their unique electronic structure enables double the electrochemical adsorption and desorption of hydrogen for Pt nanoparticles supported on CNTs in comparison with nanoparticles supported on carbon black [82]. The exchange current density on Pt/CNT electrode is about one order larger than that of commercial Pt/C even though the Pt loading is much lower in the CNT sample than that in active carbon sample [92]. Moreover, the Pt/CNT composites possess higher catalytic activity both for methanol oxidation and for oxygen reduction reaction. The enhancement of catalytic activity is attributed to the larger surface area of CNTs and the decrease in the overpotential for both reactions. Besides, SWCNTs and MWCNTs exhibit quite different behavior as the catalyst support for fuel cells [153]. Ramesh et al. found that Pt/SWCNT thin film layer allows efficient proton transfer, but the mass transfer limits power output and decreases the specific mass activity. Addition of MWCNTs could improve the mass transport within the catalyst layer and increase the mass activity.

In addition to the conductivity improvement of CNTs in the composites, the presence of CNTs during the formation of Pt nanoparticles is beneficial to obtain uniform Pt nanoparticles by providing more heterogeneous nucleation centers [154]. Then, by rational design of the structure of the exposed facets, the catalytic

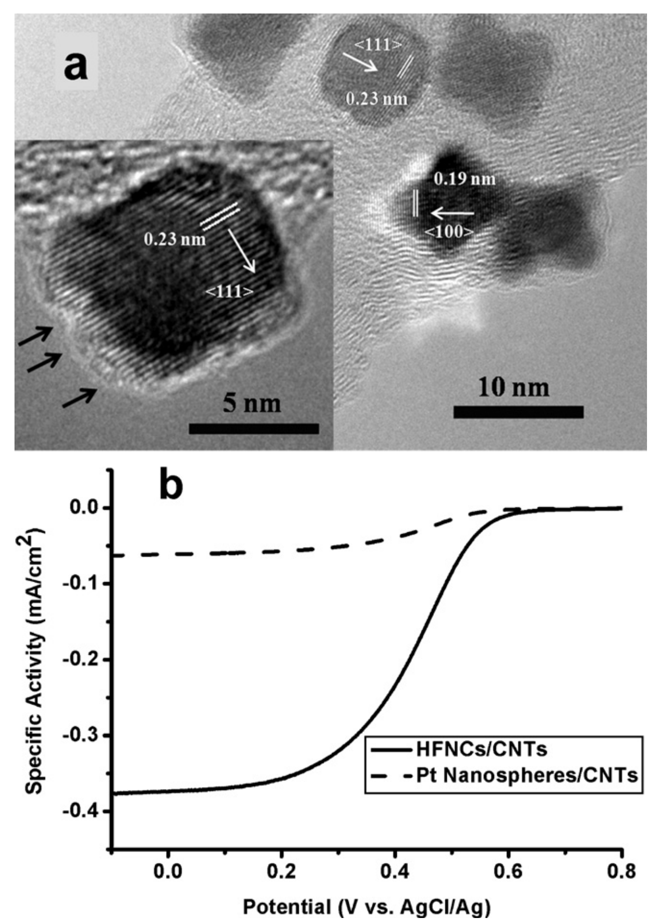

Fig. 17. (a) HRTEM images of highly faceted Pt nanocrystals (HFNCs) supported on CNTs, the inset shows the atomic steps indicated by the arrows. (b) The specific activity curves of HFNCs/CNTs and Pt nanospheres/CNTs with a scanning rate of 5 mV/s in O_2-saturated $HClO_4$ solution (0.1 M), the rotation speed is 1600 rpm.
Reproduced from Ref. [154] with permission of the Royal Society of Chemistry.

performance can be further enhanced. Introducing atomic steps to the {1 1 1} facets of Pt nanocrystals will improve the oxygen absorption ability in $HClO_4$ media. The faceted platinum nanocrystals in such morphology supported on CNTs shows 5 times higher specific activity for oxygen reduction reaction than that of Pt nanospheres supported on CNTs. Fig. 17 shows the HRTEM image of the highly faceted Pt nanocrystals (HFNCs) supported on CNTs and the corresponding specific activity curves in 0.1 M $HClO_4$ solution [154].

In summary, CNT–supported metal nanoparticles are able to satisfy the two requirements of the catalysts for electrode reactions in PEMFCs and DMFCs, i.e., improving the catalytic activity and reducing the metal loading. Therefore, metal nanocrystal/CNT composites have great potential in the fuel cell field.

4.2.2. Solar cells (solar energy conversion)

CNTs can be directly used as the energy conversion materials in solar cells, serving as both photogeneration sites and charge carriers in collecting/transport layer [155]. Introducing semiconductor nanocrystals of tunable bandgap into the system may show better promise. Semiconductor nanocrystal/CNT composites, such as CdS/CNT, CdSe/CNT, TiO_2/CNT and Cu_2S/CNT, have shown better performance in solar cells [156]. The high aspect ratio, large surface area, and high conductivity of nanotubes are beneficial for exciton dissociation and charge carrier transport in the composites thus improving the power conversion efficiency.

Transient absorption spectroscopy of CdS/SWCNT composites detects a fast electron transfer from excited CdS into the SWCNTs. This indicates that the composites may find applications in light-harvesting devices [157]. The CdS/SWCNT hybrids show very high efficiency in photocurrent generation with high quantum yield [158]. The length of SWCNTs plays a key role in resulting photocurrents and the defects in the SWCNT may affect the extent of charge separation after the photoexcitation of CdS nanoparticles.

Hu et al. have quantitatively studied the charge transfer between CdSe nanoparticles and SWCNTs using both fluorescence quenching experiments and transistor measurements [156]. CdSe nanoparticles are linked to the surfaces of SWCNTs by a kind of pyrene derivative which can adsorb on SWCNTs through π–π interactions and bind onto the CdSe nanoparticles through Cd–S bonds. The magnitude of the charge transfer possesses a strong dependency both on the light intensity and wavelength. The SWCNTs act as electron acceptors and the CdSe nanoparticles act as electron donors.

As stated above, in solar energy conversion process, the semiconductor nanoparticles normally act as electron donors and CNTs act as the electron acceptors and charge carriers. The unique structure and high conductivity make CNTs superior materials for solar cells.

4.3. Chemical sensors

Chemical sensors have important applications in environmental monitoring, chemical process controlling, as well as in agricultural and biomedical fields. CNTs have shown high sensitivity towards many gases, such as O_2, NH_3 and NO_2. Adsorption of electron withdrawing or donating molecules on CNTs will cause charge transfer either from or to CNTs, which may result in dramatic conductance change of semiconducting SWCNTs [110]. This change in conductance enables the detection of some gases even in low concentration. Molecular sensing requires strong interaction between sensors and target molecules. However, many gaseous molecules, including H_2 and CO, are not sensitive with CNTs. Decoration of CNTs with inorganic nanocrystals provides possibilities for chemically sensing more molecules.

In 2001, Kong et al. modified surface-grown SWCNTs with Pd nanoparticles using electron-beam evaporation [110]. The Pd nanoparticle/SWCNT composites are able to detect small concentrations of H_2 (as small as 4 ppm) in air and the change in conductance of SWCNTs is highly reversible. It is believed that the dissolution of atomic hydrogen in Pd nanoparticles and the charge transfer between Pd nanoparticles and SWCNTs play major roles in the sensing mechanism. In this case, SWCNTs act as molecular nanowires and the sensitivity towards H_2 is mainly attributed to Pd.

A study on the sensitivity of a series of different metal nanocrystals decorated on CNTs towards the detection of a randomized series of toxic/combustible gases, such as H_2, CH_4, CO and H_2S, shows that the thickness of the deposited metal layer has a significant effect [113]. Increasing metal thickness results in a decrease of sensitivity of the sensor devices. Too thick metal layer may even cause an electrical shorting of the devices.

4.4. Electroanalysis

Due to the large electrochemical active areas, fast electron transfer velocity and easiness in being modified with a wide range of chemical molecules and bio-molecules, inorganic nanocrystals have shown strong potential in applications in high sensitivity electroanalysis [159]. CNTs possess the advantages of large surface area, high conductivity, fast carrier transfer velocity, good electrochemical activity and fast responsive velocity. Moreover, CNTs have wide electrochemical windows, i.e., long-term stability below +2 V. And CNTs are also easy to be modified by bio-molecules. Therefore the combination of inorganic nanocrystals and CNTs not only integrates the advantages of both materials, but also enables a synergistic effect between the two materials and results in better electroanalytical performance [159].

The composites consisting of SWCNTs and platinum nanocrystals with a size of 2–3 nm exhibit remarkably improved sensitivity toward the detection of hydrogen peroxide (Fig. 18) [159]. The detection limit of the composites is 25 nM, while the detection limits of platinum nanocrystals and SWCNTs are 1.5 μM and 150 μM, respectively. Besides, these composites present a large linear response range from 25 nM to 10 μM and also from 100 μM to 2 mM for the detection of hydrogen peroxide. Biosensors composed of glucose oxidase-modified Pt nanocrystal/SWCNT composites respond more sensitively to glucose than the electrode modified with Pt nanocrystals or CNTs alone. Furthermore, the cholesterol oxidase-modified CNT–Pt electrodes show high sensitivity (with a detection limit of 1.4×10^{-6} mol/L) and very rapid electrochemical response (<20 s) towards cholesterol [160]. This kind of biosensor is stable even in detecting disassociated cholesterol in serum samples.

The electrochemical detection of trinitrotoluene (TNT) and several other nitroaromatics with metal nanoparticles (Pt, Au or Cu) on CNTs has also been investigated [161]. Due to both the excellent adsorptive properties of SWCNT and the large electroactive surface area and good electrical conductivity of Cu nanocrystals, Cu/MWCNT nanocomposites exhibit the highest synergistic signal. The detection limit of Cu/MWCNT nanocomposites for TNT is 1 ppb with linear response range up to 3 orders of magnitude. Importantly, such composites can realize the selective detection of low concentration of TNT and nitroaromatics in drinking water treatment facilities or tube wells, seawater, and contaminated soils.

4.5. Surface-enhanced Raman

Raman spectroscopy is an important and widely used methodology to characterize CNTs [162]. The standard technique generally used for probing CNTs is resonant Raman spectroscopy (RRS), which is based on the selective resonance of excitation photons coinciding with an electronic transition between the van Hove singularities of the valence band and the conduction band of SWCNTs [162].

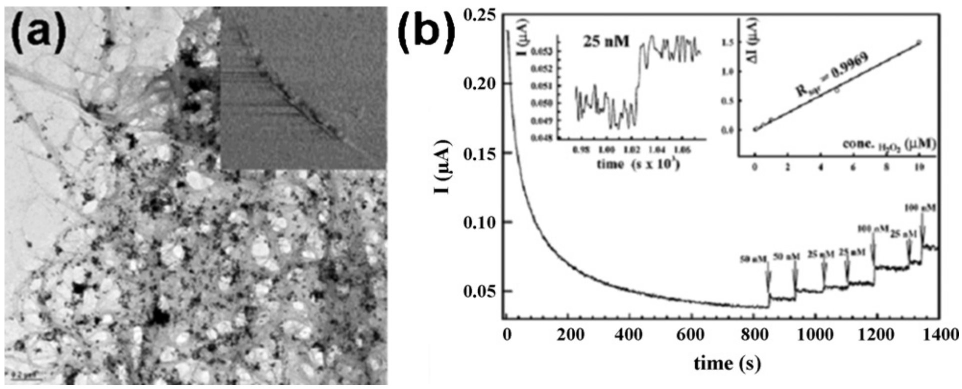

Fig. 18. (a) TEM micrograph of SWCNT in the presence of Pt nanoparticles. Inset: AFM tapping mode phase image (size, 1 µm × 1 µm; data scale, 20 nm) of one SWCNT in the presence of Pt nanoparticles. (b) Performance of GC/CNT + Pt nanoparticle electrode in amperometric detection of low concentrations of hydrogen peroxide at +0.55 V vs. Ag/AgCl (3 M NaCl). The insets show detection limit of 25 nM with S/N = 3 (left) and calibration curve for H_2O_2 concentrations between 25 nM and 10 µM (right). Reproduced from Ref. [159] with permission of the American Chemical Society.

Due to its enhanced identification, RRS can provide the detailed electronic and phonon properties of SWCNTs at the single nanotube level [163]. However, this method has its limitation that only SWCNTs in resonance with excitation photons are enhanced in Raman intensity. The Raman peaks of SWCNTs in the non-resonance regions are hardly improved by RRS because of the narrow resonance windows of SWNTs' Raman modes, of which RBM peaks are especially difficult to obtain by RRS [162]. Thus, only a very small portion of SWCNTs can be characterized using a certain excitation wavelength. This limitation has been preventing Raman spectroscopy from exhibiting the full-scale information of the SWNTs in a sample, especially for the surface-grown SWCNTs, which show extremely low Raman intensity due to the strong interaction between SWCNTs and the substrates [164,165]. Tunable laser or multi-wavelength laser system is necessary in order to obtain a comprehensive picture of any given SWCNT sample.

SERS [166,167] which is based on surface plasmon resonance (SPR) might present an alternative approach to avoid this limitation [168,169]. The surface electrons of metal nanoparticles (such as Au and Ag) can be resonant with the electrical field of incident light, resulting in strong SPR resonance in small localized regimes with strong adsorption of light. The large electric field enhancement induced by SPR results in a amplified Raman scattering signal (up to 14 orders of magnitude stronger) for nearby chemical or biological molecules. Thus, SERS has succeeded in detecting organic compounds even at single molecule level [166,167]. Therefore, SERS of CNTs, which could be realized after metal nanoparticle decoration of CNTs, can provide more detailed structural information of CNTs. Because of the high aspect ratio, stability and strong electron–phonon coupling, SWCNTs are also unique probing molecules for SERS studies. Moreover, the metal nanoparticle/CNT composites provide a good system for the investigation over the interaction between the two components.

In 2001, Li et al. coated surface-grown SWCNT samples using electron-beam evaporation to form gold nano-clusters with average diameter about 5 nm on SWCNTs [111]. Then they estimated the nanotube diameter distribution from the surface-enhanced resonant Raman spectra (SERRS) of SWCNTs by the relation between SWCNT's diameter (d) and RBM Raman shift (ω_{RBM}), $d_t = 248/\omega_{RBM}$. In this case, the diameter distribution made from SERRS only reflects the information of the nanotubes in resonance with the laser excitation energy (1.58 eV). Recently, Kumar et al. explored the similar electron-beam evaporation techniques to decorate surface-grown SWCNTs with silver nanoparticle films [114]. A lithographically patterned grid was used to locate the individual SWCNTs. Therefore, SERS enhancement factors of SWCNTs were determined unambiguously by measuring the same individual CNT before and after silver nanoparticle decoration. The SERS enhancement factor obtained by this study is up to 134,000.

By electro-depositing silver nanoparticles onto surface-grown SWCNTs, Assmus et al. have studied the effect of nanoparticle arrangement on both the enhancement magnitude and polarization dependence of Raman intensity [124]. Compared with individual silver nanoparticles, nanoparticle agglomerates Exhibit 20-fold stronger enhancement and significant distortions of the polarization characteristic. This difference is ascribed to the cavity effects within the nanoparticle agglomerates. The Raman signal is only enhanced in the range of just a few nanometers from the particle surface and decays very rapidly away from the surface. Scolari et al. also used electro-deposition method to cover individual SWCNTs with isolated gold nanoparticles with diameters from 10 nm to 120 nm for the investigation on SERS of SWCNTs [130]. As the SPR scattering of gold nanoparticle increases with the size increase of the nanoparticle, the Raman enhancement increases with increasing particle size at longer wavelengths. Furthermore, maximum Raman intensity is obtained when both nanotube and metal particle are in optical resonance.

Tong et al. have investigated the effect of the distance between the gold nanoparticles and the SWCNTs on SERS of individual SWCNTs by AFM manipulation [137]. The measured SERS enhancement strongly relies on the distance as well as the polarization angles.

The above studies primarily focused on the SERS of SWCNTs in resonance with the excitation photons. None of them demonstrated the observation of Raman peaks for every SWCNT or RBM peaks in the nonresonance regions of the surface-grown samples. Recently, an electroless method, which was comprised of seed deposition and seeded growth, has been developed to realize the decoration of every surface-grown CNTs with gold nanoparticles of controlled size and small interparticle distance [117]. High SERS activity is achieved for the gold nanoparticles with proper size, small interparticle distance and good alignment along SWCNTs. Consequently, in situ Raman detection of every surface-grown SWCNT has been realized for the first time (Fig. 19) [117]. Not only the nonresonant G band but also the nonresonant RBM band [117] of individual SWVMT can be detected. Further investigation revealed that the strong SERS enhancement mainly come from the electromagnetic SERS attributed to the coupled SPR absorption in the high-density gold nanoparticles aligned on SWCNTs [117].

4.6. Other applications

Besides the applications mentioned above, inorganic nanocrystal/carbon nanotube composites show promising applications in

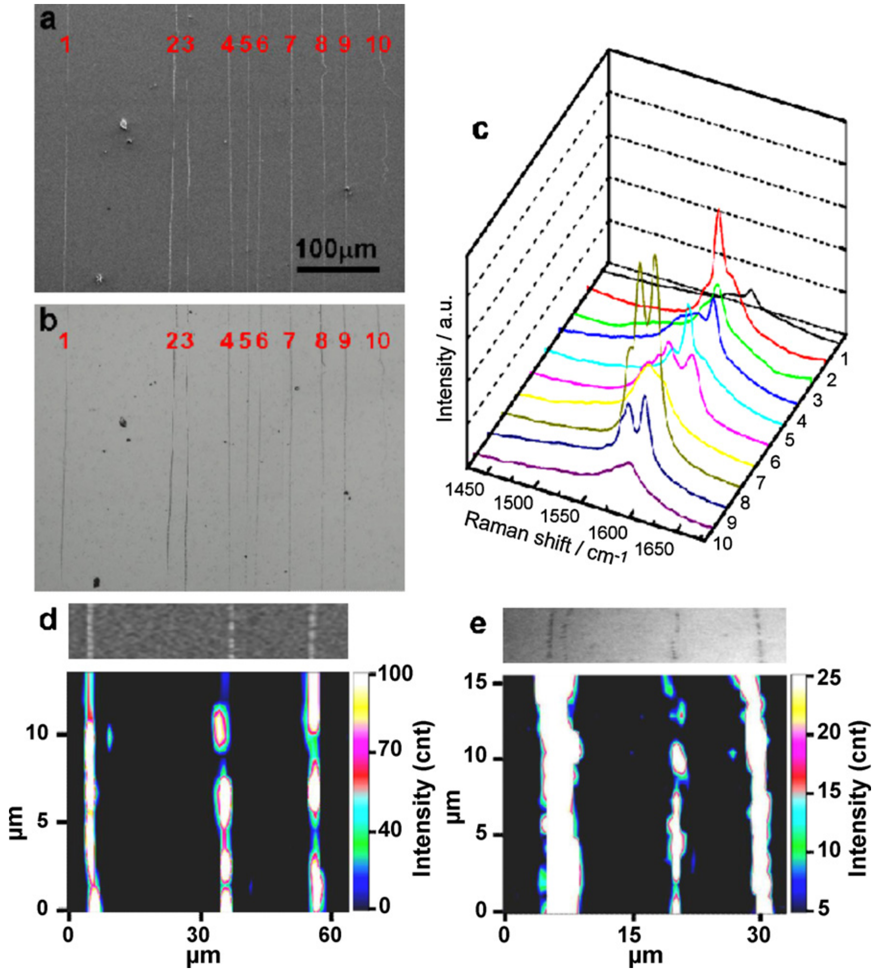

Fig. 19. SEM image (a), optical image (b), and corresponding Raman spectra (c) of 10 SWCNTs grown on SiO_x/Si after gold decoration with an excitation wavelength of 633 nm. Mapping of the Raman intensity of three SWCNTs (d) and four SWCNTs (e), respectively, in the range of 1450–1650 cm^{-1} with the corresponding SEM image (d) and optical image (e) shown above.
Reproduced from Ref. [117] with permission of the American Chemical Society.

many other areas, such as electronics [89,138,170–173], optics [174–176], hydrogen storage [177–180] and so on.

Deposition of metals onto the nanotubes can reduce the electrode/nanotube contact resistance, resulting in excellent electrical contact between the CNT and the metal electrode [138,172]. The gold nanoparticle-coated SWCNT films obtained from the electroless reduction of gold ion on SCWNT networks show a 2-fold enhancement in the electrical conductivity with a negligible loss of the optical transparency [89]. In addition, inorganic nanocrystal decorated CNTs have been investigated for their field emission properties and the possible applications in field-emitter-displays [171,173].

On the other hand, CNT–TiO_2 composites have attracted great interest for their enhanced photocatalytic properties at room temperature compared with TiO_2 alone [176]. With the excellent photocatalytic property, the CNT–TiO_2 composites may be used in the treatment of various biological, organic, or inorganic hazardous pollutants in both water and air. The stimuli-responsive optoelectronics devices from individual SWCNT transistor coated with photoactive TiO_2 quantum dots show a photoswitching effect. The p-type semiconducting carbon nanotubes show fast significant current decrease under UV irradiation and excellent reversibility when the UV light is switched off. However the ambipolar tubes show the mirror-image of p-type semiconducting tubes when different gate bias voltages are applied [175].

5. Conclusion

CNTs combining with inorganic nanomaterials bring about a family of composite materials with extraordinary properties. Intensive studies have been carried out and much progress has been achieved in the preparation and application of CNT–supported inorganic nanomaterials. However, there are still many challenges. The controlled preparation of inorganic nanomaterial/CNT composites with superior function is the foundation for further applications. For the controlled preparation, the conflicts and balance between maintaining the original structure and properties of CNTs and introducing anchoring sites into CNTs by modification, the shape and structure control of nanocrystals deposited on CNTs, and the site-defined deposition of nanocrystals on CNTs are some of the remaining important issues. Inorganic nanomaterial/CNT composites have already shown great potential in the areas of catalysis, energy conversion, analytical technology, etc. It is expected that this kind of material will play very important roles in solving the energy and environmental problems in the future.

Acknowledgements

The authors would like to acknowledge funding support from National Natural Science Foundation (Projects 50772002 and

90406018), and Ministry of Science and Technology (Projects 2006CB932403, 2007CB936202, and 2006CB932701) of China.

References

[1] R. Saito, M.S. Dresselhaus, G. Dresselhaus, Physical Properties of Carbon Nanotubes, World Scientific Publishing, Singapore, 1998.
[2] P.G. Collins, P. Avouris, Sci. Am. 283 (2000) 62.
[3] S. Iijima, Nature 354 (1991) 56.
[4] P. Avouris, Acc. Chem. Res. 35 (2002) 1026.
[5] H.J. Dai, Acc. Chem. Res. 35 (2002) 1035.
[6] M. Ouyang, J.L. Huang, C.M. Lieber, Acc. Chem. Res. 35 (2002) 1018.
[7] P.L. McEuen, J.Y. Park, MRS Bull. 29 (2004) 272.
[8] H. Rafii-Tabar, Phys. Rep. 390 (2004) 235.
[9] M.F. Yu, J. Eng. Mater. Technol. 126 (2004) 271.
[10] P. Sharma, P. Ahuja, Mater. Res. Bull. 43 (2008) 2517.
[11] C.N.R. Rao, C.A.K. Müller Achim, The Chemistry of Nanomaterials: Synthesis, Properties and Applications, John Wiley, 2004.
[12] G.G. Wildgoose, C.E. Banks, R.G. Compton, Small 2 (2006) 182.
[13] V. Georgakilas, D. Gournis, V. Tzitzios, L. Pasquato, D.M. Guldi, M. Prato, J. Mater. Chem. 17 (2007) 2679.
[14] X.G. Hu, S.J. Dong, J. Mater. Chem. 18 (2008) 1279.
[15] D. Vairavapandian, P. Vichchulada, M.D. Lay, Anal. Chim. Acta 626 (2008) 119.
[16] X. Peng, J. Chen, J.A. Misewich, S.S. Wong, Chem. Soc. Rev. 38 (2009) 1076.
[17] T.W. Ebbesen, P.M. Ajayan, Nature 358 (1992) 220.
[18] C. Journet, W.K. Maser, P. Bernier, A. Loiseau, M.L. delaChapelle, S. Lefrant, P. Deniard, R. Lee, J.E. Fischer, Nature 388 (1997) 756.
[19] A. Thess, R. Lee, P. Nikolaev, H.J. Dai, P. Petit, J. Robert, C.H. Xu, Y.H. Lee, S.G. Kim, A.G. Rinzler, D.T. Colbert, G.E. Scuseria, D. Tomanek, J.E. Fischer, R.E. Smalley, Science 273 (1996) 483.
[20] Z.F. Ren, Z.P. Huang, J.W. Xu, J.H. Wang, P. Bush, M.P. Siegal, P.N. Provencio, Science 282 (1998) 1105.
[21] S.S. Fan, M.G. Chapline, N.R. Franklin, T.W. Tombler, A.M. Cassell, H.J. Dai, Science 283 (1999) 512.
[22] C. Bower, O. Zhou, W. Zhu, D.J. Werder, S.H. Jin, Appl. Phys. Lett. 77 (2000) 2767.
[23] M. Su, B. Zheng, J. Liu, Chem. Phys. Lett. 322 (2000) 321.
[24] M.L. Terranova, V. Sessa, M. Rossi, Chem. Vap. Depos. 12 (2006) 315.
[25] H. Yokomichi, F. Sakai, M. Ichihara, N. Kishimoto, Phys. B: Condens. Matter 323 (2002) 311.
[26] R. Vajtai, K. Kordas, B.Q. Wei, J. Bekesi, S. Leppavuori, T.F. George, P.M. Ajayan, Mater. Sci. Eng. C 19 (2002) 271.
[27] A.Y. Cao, L.J. Ci, D.J. Li, B.Q. Wei, C.L. Xu, J. Liang, D.H. Wu, Chem. Phys. Lett. 335 (2001) 150.
[28] Y. Zhang, W.W. Zhou, Z. Jin, L. Ding, Z.Y. Zhang, X.I. Liang, Y. Li, Chem. Mater. 20 (2008) 7521.
[29] W.W. Zhou, Z.Y. Han, J.Y. Wang, Y. Zhang, Z. Jin, X. Sun, Y.W. Zhang, C.H. Yan, Y. Li, Nano Lett. 6 (2006) 2987.
[30] C.J. Lee, S.C. Lyu, H.W. Kim, C.Y. Park, C.W. Yang, Chem. Phys. Lett. 359 (2002) 109.
[31] E. Couteau, K. Hernadi, J.W. Seo, L. Thien-Nga, C. Miko, R. Gaal, L. Forro, Chem. Phys. Lett. 378 (2003) 9.
[32] P. Nikolaev, M.J. Bronikowski, R.K. Bradley, F. Rohmund, D.T. Colbert, K.A. Smith, R.E. Smalley, Chem. Phys. Lett. 313 (1999) 91.
[33] H.J. Dal, A.G. Rinzler, P. Nikolaev, A. Thess, D.T. Colbert, R.E. Smalley, Chem. Phys. Lett. 260 (1996) 471.
[34] Z. Jin, H.B. Chu, J.Y. Wang, J.X. Hong, W.C. Tan, Y. Li, Nano Lett. 7 (2007) 2073.
[35] A. Javey, H.J. Dai, J. Am. Chem. Soc. 127 (2005) 11942.
[36] L. Ding, W.W. Zhou, H.B. Chu, Z. Jin, Y. Zhang, Y. Li, Chem. Mater. 18 (2006) 4109.
[37] E. Joselevich, C.M. Lieber, Nano Lett. 2 (2002) 1137.
[38] Y.G. Zhang, A.L. Chang, J. Cao, Q. Wang, W. Kim, Y.M. Li, N. Morris, E. Yenilmez, J. Kong, H.J. Dai, Appl. Phys. Lett. 79 (2001) 3155.
[39] S.M. Huang, X.Y. Cai, J. Liu, J. Am. Chem. Soc. 125 (2003) 5636.
[40] S.M. Huang, M. Woodson, R. Smalley, J. Liu, Nano Lett. 4 (2004) 1025.
[41] A. Ismach, L. Segev, E. Wachtel, E. Joselevich, Angew. Chem. Int. Ed. 43 (2004) 6140.
[42] S. Han, X.L. Liu, C.W. Zhou, J. Am. Chem. Soc. 127 (2005) 5294.
[43] C. Kocabas, S.H. Hur, A. Gaur, M.A. Meitl, M. Shim, J.A. Rogers, Small 1 (2005) 1110.
[44] C. Kocabas, M. Shim, J.A. Rogers, J. Am. Chem. Soc. 128 (2006) 4540.
[45] L. Ding, D.N. Yuan, J. Liu, J. Am. Chem. Soc. 130 (2008) 5428.
[46] W. Zhou, L. Ding, J. Liu, Nano Res. 2 (2009) 593.
[47] T.P. McNicholas, L. Ding, D.N. Yuan, J. Liu, Nano Lett. 9 (2009) 3646.
[48] N. Ishigami, H. Ago, K. Imamoto, M. Tsuji, K. Iakoubovskii, N. Minami, J. Am. Chem. Soc. 130 (2008) 9918.
[49] I.W. Chiang, R.E. Smalley, J.L. Margrave, R.H. Hauge, J. Phys. Chem. B 106 (2001) 1157.
[50] T. Tohji, H. Takahashi, Y. Shinoda, N. Shimizu, B. Jeyadevan, I. Matsuoka, Y. Saito, A. Kasuya, T. Ohsuna, K. Hiraga, Y. Nishina, Nature 383 (1996) 679.
[51] E.E. Dujardin, A. Krishnan, M.M.J. Treacy, Adv. Mater. 10 (1998) 611.
[52] H.Y. Xu, R.H. Hauge, R.E. Smalley, Nano Lett. 5 (2005) 163.
[53] H.T. Fang, C.G. Liu, C. Liu, F. Li, M. Liu, H.M. Cheng, Chem. Mater. 16 (2004) 5744.
[54] C.J. Murphy R., M. Cadek, B. McCarthy, M. Bent, A. Drury, et al., J. Phys. Chem. B 106 (2002) 3087.
[55] K. Shen, S. Curran, Huifang Xu, Snezna Rogelj, Yingbing Jiang, James Dewald, Tanja Pietrass, J. Phys. Chem. B 109 (2005) 4455.
[56] A.G. Liu, H. Dai, J.H. Hafner, R.K. Bradley, P.J. Boul, A. Lu, T. Iverson, K. Shelimov, C.B. Huffman, F. Rodriguez-Macias, Y.-S. Shon, T.R. Lee, D.T. Colbert, R.E. Smalley, Science 280 (1998) 1253.
[57] M.A. Chen, H. Hu, Y. Chen, A.M. Rao, P.C. Eklund, R.C. Haddon, Science 282 (1998) 95.
[58] W. Fu, Y. Lin, L.A. Riddle, D.L. Carroll, Y.-P. Sun, Nano Lett. 1 (2001) 439.
[59] M.E. Kamaras, H. Hu, B. Zhao, R.C. Haddon, Science 301 (2003) 1501.
[60] C.A. Strano, M.L. Usrey, P.W. Barone, M.J. Allen, H. Shan, C. Kittrell, R.H. Hauge, J.M. Tour, R.E. Smalley, T.W. Dujardin, A. Ebbesen, M. Krishnan, M.J. Treacy, Science 301 (2003) 1519.
[61] A. Zheng, E.D. Semke, B.A. Diner, R.S. McLean, S.R. Lustig, R.E. Richardson, N.G. Tassi, Nat. Mater. 2 (2003) 338.
[62] Y. Chen, D. Wang, H. Dai, J. Am. Chem. Soc. 123 (2002) 3838.
[63] J.-O. Besteman, F.G.M. Wiertz, H.A. Heering, C. Dekker, Nano Lett. 3 (2003) 727.
[64] M.S. Moore, E.H. Haroz, R.H. Hauge, R.E. Smalley, J. Schmidt, Y. Talmon, Nano Lett. 3 (2003) 1379.
[65] A. Fukushima, Y. Ishimura, T. Yamamoto, T. Takigawa, N. Ishii, T. Aida, Science 300 (2003) 2072.
[66] H.C.J. Wang, Y. Li, ACS Nano 2 (2008) 2540.
[67] J.Y. Wang, Y. Li, J. Am. Chem. Soc. 131 (2009) 5364.
[68] L.D. Zhang, J.M. Mou, Nanomaterials and Nanostructures, Science Press, Beijing, 2001.
[69] K.S. Coleman, S.R. Bailey, S. Fogden, M.L.H. Green, J. Am. Chem. Soc. 125 (2003) 8722.
[70] M.A. Correa-Duarte, J. Perez-Juste, A. Sanchez-Iglesias, M. Giersig, L.M. Liz-Marzan, Angew. Chem. Int. Ed. 44 (2005) 4375.
[71] C.Q. Li, Z. Jin, H.B. Chu, Y. Li, J. Nanosci. Nanotechnol. 8 (2008) 4441.
[72] L. Liu, T.X. Wang, J.X. Li, Z.X. Guo, L.M. Dai, D.Q. Zhang, D.B. Zhu, Chem. Phys. Lett. 367 (2003) 747.
[73] L. Han, W. Wu, F.L. Kirk, J. Luo, M.M. Maye, N.N. Kariuki, Y.H. Lin, C.M. Wang, C.J. Zhong, Langmuir 20 (2004) 6019.
[74] J. Li, S.B. Tang, L. Lu, H.C. Zeng, J. Am. Chem. Soc. 129 (2007) 9401.
[75] B.F. Pan, D.X. Cui, C.S. Ozkan, M. Ozkan, P. Xu, T. Huang, F.T. Liu, H. Chen, Q. Li, R. He, F. Gao, J. Phys. Chem. C 112 (2008) 939.
[76] Y.L. Hsin, K.C. Hwang, C.T. Yeh, J. Am. Chem. Soc. 129 (2007) 9999.
[77] C. Klinke, J.B. Hannon, A. Afzali, P. Avouris, Nano Lett. 6 (2006) 906.
[78] J.M. Planeix, N. Coustel, B. Coq, V. Brotons, P.S. Kumbhar, R. Dutartre, P. Geneste, P. Bernier, P.M. Ajayan, J. Am. Chem. Soc. 116 (1994) 7935.
[79] B.H. Juarez, C. Klinke, A. Kornowski, H. Weller, Nano Lett. 7 (2007) 3564.
[80] F. Gu, C.Z. Li, S.F. Wang, Inorg. Chem. 46 (2007) 5343.
[81] W.Q. Han, A. Zettl, Nano Lett. 3 (2003) 681.
[82] Y.C. Xing, J. Phys. Chem. B 108 (2004) 19255.
[83] B.H. Wu, D. Hu, Y.J. Kuang, B. Liu, X.H. Zhang, J.H. Chen, Angew. Chem. Int. Ed. 48 (2009) 4751.
[84] Y. Zhang, H.J. Dai, Appl. Phys. Lett. 77 (2000) 3015.
[85] Y. Zhang, N.W. Franklin, R.J. Chen, H.J. Dai, Chem. Phys. Lett. 331 (2000) 35.
[86] W.J. Huang, H. Chen, J.M. Zuo, Small 2 (2006) 1418.
[87] H.T. Yu, X. Quan, S. Chen, H.M. Zhao, J. Phys. Chem. C 111 (2007) 12987.
[88] D.S. Kim, T. Lee, K.E. Geckeler, Angew. Chem. Int. Ed. 45 (2006) 104.
[89] B.S. Kong, D.H. Jung, S.K. Oh, C.S. Han, H.T. Jung, J. Phys. Chem. C 111 (2007) 8377.
[90] C. Wang, M. Waje, X. Wang, J.M. Tang, R.C. Haddon, Y.S. Yan, Nano Lett. 4 (2004) 345.
[91] X.R. Ye, Y.H. Lin, C.M. Wang, C.M. Wai, Adv. Mater. 15 (2003) 316.
[92] Y.H. Lin, X.L. Cui, C. Yen, C.M. Wai, J. Phys. Chem. B 109 (2005) 14410.
[93] Z.Y. Sun, Z.M. Liu, B.X. Han, Y. Wang, J.M. Du, Z.L. Xie, G.J. Han, Adv. Mater. 17 (2005) 928.
[94] Z.M. Liu, B.X. Han, Adv. Mater. 20 (2008) 1.
[95] Y. Wang, X. Xu, Z.Q. Tian, Y. Zong, H.M. Cheng, C.J. Lin, Chem. Eur. J. 12 (2006) 2542.
[96] B. Xue, P. Chen, Q. Hong, J. Lin, K.L. Tan, J. Mater. Chem. 11 (2001) 2378.
[97] C.Q. Li, N.J. Sun, J.F. Ni, J.Y. Wang, H.B. Chu, H.H. Zhou, M.X. Li, Y. Li, J. Solid State Chem. 181 (2008) 2620.
[98] B.H. Juarez, M. Meyns, A. Chanaewa, Y.X. Cai, C. Klinke, H. Weller, J. Am. Chem. Soc. 130 (2008) 15282.
[99] H. Lee, S.W. Yoon, E.J. Kim, J. Park, Nano Lett. 7 (2007) 778.
[100] N. Du, H. Zhang, B. Chen, J.B. Wu, X.Y. Ma, Z.H. Liu, Y.Q. Zhang, D. Yang, X.H. Huang, J.P. Tu, Adv. Mater. 19 (2007) 4505.
[101] N. Du, H. Zhang, B.D. Chen, X.Y. Ma, Z.H. Liu, J.B. Wu, D.R. Yang, Adv. Mater. 19 (2007) 1641.
[102] N.D. Hoa, N. Van Quy, H. Song, Y. Kang, Y. Cho, D. Kim, J. Cryst. Growth 311 (2009) 657.
[103] Y.S. Min, E.J. Bae, K.S. Jeong, Y.J. Cho, J.H. Lee, W.B. Choi, G.S. Park, Adv. Mater. 15 (2003) 1019.
[104] Z.Y. Sun, H.Q. Yuan, Z.M. Liu, B.X. Han, X.R. Zhang, Adv. Mater. 17 (2005) 2993.
[105] C.N.R. Rao, B.C. Satishkumar, A. Govindaraj, Chem. Commun. (1997) 1581.
[106] M.P. Anantram, F. Leonard, Rep. Prog. Phys. 69 (2006) 507.
[107] P. Avouris, Z.H. Chen, V. Perebeinos, Nat. Nanotechnol. 2 (2007) 605.
[108] P. Bertoncello, J.P. Edgeworth, J.V. Macpherson, P.R. Unwin, J. Am. Chem. Soc. 129 (2007) 10982.

[109] J. Kong, N.R. Franklin, C.W. Zhou, M.G. Chapline, S. Peng, K.J. Cho, H.J. Dai, Science 287 (2000) 622.
[110] J. Kong, M.G. Chapline, H.J. Dai, Adv. Mater. 13 (2001) 1384.
[111] Y.M. Li, W. Kim, Y.G. Zhang, M. Rolandi, D.W. Wang, H.J. Dai, J. Phys. Chem. B 105 (2001) 11424.
[112] B.K. Kim, N. Park, P.S. Na, H.M. So, J.J. Kim, H. Kim, K.J. Kong, H. Chang, B.H. Ryu, Y.M. Choi, J.O. Lee, Nanotechnology 17 (2006) 496.
[113] A. Star, V. Joshi, S. Skarupo, D. Thomas, J.C.P. Gabriel, J. Phys. Chem. B 110 (2006) 21014.
[114] R. Kumar, H. Zhou, S.B. Cronin, Appl. Phys. Lett. 91 (2007) 223105.
[115] H.C. Choi, M. Shim, S. Bangsaruntip, H.J. Dai, J. Am. Chem. Soc. 124 (2002) 9058.
[116] A.J. Mieszawska, R. Jalilian, G.U. Sumanasekera, F.P. Zamborini, J. Am. Chem. Soc. 127 (2005) 10822.
[117] H.B. Chu, J.Y. Wang, L. Ding, D.N. Yuan, Y. Zhang, J. Liu, Y. Li, J. Am. Chem. Soc. 131 (2009) 14310.
[118] Y. Lee, H.J. Song, H.S. Shin, H.J. Shin, H.C. Choi, Small 1 (2005) 975.
[119] L.T. Qu, L.M. Dai, J. Am. Chem. Soc. 127 (2005) 10806.
[120] T.M. Day, P.R. Unwin, N.R. Wilson, J.V. Macpherson, J. Am. Chem. Soc. 127 (2005) 10639.
[121] Y.W. Fan, B.R. Goldsmith, P.G. Collins, Nat. Mater. 4 (2005) 906.
[122] B.M. Quinn, C. Dekker, S.G. Lemay, J. Am. Chem. Soc. 127 (2005) 6146.
[123] B.M. Quinn, S.G. Lemay, Adv. Mater. 18 (2006) 855.
[124] T. Assmus, K. Balasubramanian, M. Burghard, K. Kern, M. Scolari, N. Fu, A. Myalitsin, A. Mews, Appl. Phys. Lett. 90 (2007) 173109.
[125] Y.C. Chen, R.J. Young, J.V. Macpherson, N.R. Wilson, J. Phys. Chem. C 111 (2007) 16167.
[126] D.R. Kauffman, A. Star, Nano Lett. 7 (2007) 1863.
[127] S. Mubeen, T. Zhang, B. Yoo, M.A. Deshusses, N.V. Myung, J. Phys. Chem. C 111 (2007) 6321.
[128] S.M. Huang, Y. Qian, J.Y. Chen, Q.R. Cai, L. Wan, S. Wang, W.B. Hu, J. Am. Chem. Soc. 130 (2008) 11860.
[129] P. Qian, Z.Y. Wu, P. Diao, G.M. Zhang, J. Zhang, Z.F. Liu, J. Phys. Chem. C 112 (2008) 13346.
[130] M. Scolari, A. Mews, N. Fu, A. Myalitsin, T. Assmus, K. Balasubramanian, M. Burghard, K. Kern, J. Phys. Chem. C 112 (2008) 391.
[131] L. Marty, A.M. Bonnot, A. Bonhomme, A. Iaia, C. Naud, E. Andre, V. Bouchiat, Small 2 (2006) 110.
[132] C. Warakulwit, T. Nguyen, J. Majimel, M.H. Delville, V. Lapeyre, P. Garrigue, V. Ravaine, J. Limtrakul, A. Kuhn, Nano Lett. 8 (2008) 500.
[133] J.G. Duque, M. Pasquali, H.K. Schmidt, J. Am. Chem. Soc. 130 (2008) 15340.
[134] M.S. Raghuveer, A. Kumar, M.J. Frederick, G.P. Louie, P.G. Ganesan, G. Ramanath, Adv. Mater. 18 (2006) 547.
[135] C. Thelander, M.H. Magnusson, K. Deppert, L. Samuelson, P.R. Poulsen, J. Nygard, J. Borggreen, Appl. Phys. Lett. 79 (2001) 2106.
[136] A. Gruneis, M.J. Esplandiu, D. Garcia-Sanchez, A. Bachtold, Nano Lett. 7 (2007) 3766.
[137] L.M. Tong, Z.P. Li, T. Zhu, H.X. Xu, Z.F. Liu, J. Phys. Chem. C 112 (2008) 7119.
[138] C.P.R. Dockendorf, M. Steinlin, D. Poulikakos, T.Y. Choi, Appl. Phys. Lett. 90 (2007).
[139] H.B. Chu, Z. Jin, Y. Zhang, W.W. Zhou, L. Ding, Y. Li, J. Phys. Chem. C 112 (2008) 13437.
[140] K. Lee, J.J. Zhang, H.J. Wang, D.P. Wilkinson, J. Appl. Electrochem. 36 (2006) 507.
[141] J.M. Nhut, L. Pesant, J.P. Tessonnier, G. Wine, J. Guille, C. Pham-Huu, M.J. Ledoux, Appl. Catal. A 254 (2003) 345.
[142] X.L. Pan, Z.L. Fan, W. Chen, Y.J. Ding, H.Y. Luo, X.H. Bao, Nat. Mater. 6 (2007) 507.
[143] J.P. Tessonnier, L. Pesant, G. Ehret, M.J. Ledoux, C. Pham-Huu, Appl. Catal. A 288 (2005) 203.
[144] J.Z. Luo, L.Z. Gao, Y.L. Leung, C.T. Au, Catal. Lett. 66 (2000) 91.
[145] A.M. Zhang, J.L. Dong, Q.H. Xu, H.K. Rhee, X.L. Li, Catal. Today 93–95 (2004) 347.
[146] W. Chen, Z.L. Fan, X.L. Pan, X.H. Bao, J. Am. Chem. Soc. 130 (2008) 9414.
[147] K.E. Gubbins, E.E. Santiso, A.M. George, C.H. Turner, M.K. Kostov, M. Buongiorno-Nardelli, M. Sliwinska-Bartkowiak, Appl. Surf. Sci. 252 (2005) 766.
[148] B.C. Huang, R. Huang, D.J. Jin, D.Q. Ye, Catal. Today 126 (2007) 279.
[149] J.C. Kang, S.L. Zhang, Q.H. Zhang, Y. Wang, Angew. Chem. Int. Ed. 48 (2009) 2565.
[150] H.S. Liu, C.J. Song, L. Zhang, J.J. Zhang, H.J. Wang, D.P. Wilkinson, J. Power Sources 155 (2006) 95.
[151] W.Z. Li, C.H. Liang, W.J. Zhou, J.S. Qiu, Z.H. Zhou, G.Q. Sun, Q. Xin, J. Phys. Chem. B 107 (2003) 6292.
[152] G. Girishkumar, K. Vinodgopal, P.V. Kamat, J. Phys. Chem. B 108 (2004) 19960.
[153] P. Ramesh, M.E. Itkis, J.M. Tang, R.C. Haddon, J. Phys. Chem. C 112 (2008) 9089.
[154] Z.Y. Lin, H.B. Chu, Y.H. Shen, L. Wei, H.C. Liu, Y. Li, Chem. Commun. (2009) 7167.
[155] J.E. Trancik, S.C. Barton, J. Hone, Nano Lett. 8 (2008) 982.
[156] L. Hu, Y.L. Zhao, K. Ryu, C. Zhou, J.F. Stoddart, G. Gruner, Adv. Mater. 20 (2008) 939.
[157] I. Robel, B.A. Bunker, P.V. Kamat, Adv. Mater. 17 (2005) 2458.
[158] L. Sheeney-Haj-Khia, B. Basnar, I. Willner, Angew. Chem. Int. Ed. 44 (2005) 78.
[159] S. Hrapovic, Y.L. Liu, K.B. Male, J.H.T. Luong, Anal. Chem. 76 (2004) 1083.
[160] Q.C. Shi, T.Z. Peng, Y.N. Zhu, C.F. Yang, Electroanalysis 17 (2005) 857.
[161] S. Hrapovic, E. Majid, Y. Liu, K. Male, J.H.T. Luong, Anal. Chem. 78 (2006) 5504.
[162] M.S. Dresselhaus, G. Dresselhaus, R. Saito, A. Jorio, Phys. Rep.: Rev. Sect. Phys. Lett. 409 (2005) 47.
[163] A. Jorio, R. Saito, J.H. Hafner, C.M. Lieber, M. Hunter, T. McClure, G. Dresselhaus, M.S. Dresselhaus, Phys. Rev. Lett. 86 (2001) 1118.
[164] Y.Y. Zhang, J. Zhang, H.B. Son, J. Kong, Z.F. Liu, J. Am. Chem. Soc. 127 (2005) 17156.
[165] Y.Y. Zhang, H. Son, J. Zhang, M.S. Dresselhaus, J. Kong, Z.F. Liu, J. Phys. Chem. C 111 (2007) 1983.
[166] K. Kneipp, Y. Wang, H. Kneipp, L.T. Perelman, I. Itzkan, R. Dasari, M.S. Feld, Phys. Rev. Lett. 78 (1997) 1667.
[167] K. Kneipp, H. Kneipp, J. Kneipp, Acc. Chem. Res. 39 (2006) 443.
[168] K. Kneipp, H. Kneipp, P. Corio, S.D.M. Brown, K. Shafer, J. Motz, L.T. Perelman, E.B. Hanlon, A. Marucci, G. Dresselhaus, M.S. Dresselhaus, Phys. Rev. Lett. 84 (2000) 3470.
[169] D. Takagi, Y. Homma, H. Hibino, S. Suzuki, Y. Kobayashi, Nano Lett. 6 (2006) 2642.
[170] K. Jurkschat, S.J. Wilkins, C.J. Salter, H.C. Leventis, G.G. Wildgoose, L. Jiang, T.G.J. Jones, A. Crossley, R.G. Compton, Small 2 (2006) 95.
[171] K. Kim, S.H. Lee, W. Yi, J. Kim, J.W. Choi, Y. Park, J.H. Jin, Adv. Mater. 15 (2003) 1618.
[172] D.W. Austin, A.A. Puretzky, D.B. Geohegan, P.F. Britt, M.A. Guillorn, M.L. Simpson, Chem. Phys. Lett. 361 (2002) 525.
[173] C.S. Huang, C.Y. Yeh, Y.H. Chang, Y.M. Hsieh, C.Y. Ku, Q.T. Lai, Diamond Relat. Mater. 18 (2009) 452.
[174] S. Chaudhary, J.H. Kim, K.V. Singh, M. Ozkan, Nano Lett. 4 (2004) 2415.
[175] S. Liu, J.M. Li, Q. Shen, Y. Cao, X.F. Guo, G.M. Zhang, C.Q. Teng, J. Zhang, Z.F. Liu, M.L. Steigerwald, D.S. Xu, C. Nuckolls, Angew. Chem. Int. Ed. 48 (2009) 4759.
[176] K. Woan, G. Pyrgiotakis, W. Sigmund, Adv. Mater. 21 (2009) 2233.
[177] L. Weixue, H. Sumei, H. Yuan, D. Jianfeng, W. Qing, X. Yingge, Int. J. Mod. Phys. B (2009) 1358.
[178] S.P. Yi, H.Y. Zhang, L. Pei, Y.J. Zhu, X.L. Chen, X.M. Xue, J. Alloys Compd. 420 (2006) 312.
[179] Z.X. Yu, H.F. Sun, E.D. Wang, J. Liang, W.B. Fang, Chin. J. Nonferr. Met. 15 (2005) 876.
[180] H.S. Kim, H. Lee, K.S. Han, J.H. Kim, M.S. Song, M.S. Park, J.Y. Lee, J.K. Kang, J. Phys. Chem. B 109 (2005) 8983.